3rd International Symposium on Integrating CFD and Experiments in Aerodynamics
20-21 June 2007
U.S. Air Force Academy, CO, USA

EXPERIMENTAL AND NUMERICAL INVESTIGATION OF FLOW AND HEAT TRANSFER IN A RIBBED SQUARE DUCT

T. Arts
C. Benocci
P. Rambaud

von Karman Institute for Fluid Dynamics
72 Chaussée de Waterloo
B-1640 Rhode-Saint-Genèse, Belgium
arts@vki.ac.be, benocci@vki.ac.be, rambaud@vki.ac.be

Abstract

The present contribution describes the methodology and results of an experimental/numerical research program progressing at the von Karman Institute about the investigation of flow and heat transfer in a square section stationary duct equipped with high blockage ribs on one face. This geometry is representative of a high pressure turbine blade cooling channel. The purpose is to highlight the interaction and the synergy between experimental and simulation approaches. The paper shows how the experimental results lead to a conceptual model of the behavior and the topology of this flow. A numerical prediction of the flow over a single rib, obtained from a Large-Eddy Simulation, is able to validate this model, to provide additional information eventually not accessible by the experiments and to put in evidence the underlying structures driving the process. Simulations of a multi-rib domain put in evidence the possible existence of flow structures longer than one rib-pitch length and suggest possible avenues of futures experimental/numerical campaigns to gain a full understanding of this class of flows.

Key words: internal cooling of turbine blades, ribbed ducts, PIV, infra-red thermography, LES

Introduction

The efficiency of a jet engine turbine can be improved mainly by increasing its inlet temperature. However, in most of the current applications, this temperature is above the melting point temperature of the blade and end-wall material and an efficient blade cooling has to be applied to avoid any catastrophic failure. Internal convection cooling is a common technique used for this purpose. As the heat transfer between the walls of the cooling channel and the coolant evidently depends on the topology of the mean flow and on the level of turbulence, the cooling efficiency is therefore significantly influenced by the geometry of the duct via its effects on the flow-field. Therefore, the internal cooling of a blade can be augmented by using turbulence generators such as ribs, pin fins, dimples … installed on the wall(s) of the cooling duct. The obvious drawback associated with the use of these obstacles is that while they enhance turbulence and turbulent heat transfer they also increase the pressure drop, so that advantages and disadvantages of this approach must accurately be assessed and tuned.

This research topic has been intensely addressed at the von Karman Institute for Fluid Dynamics (VKI) by experimental means since the late 90s, when a first dedicated experimental facility was designed and built. Rau et al. [1, 2] applied Laser Doppler Velocimetry (LDV) and Liquid Crystal Thermometry (LCT) to investigate the flow field and the heat transfer respectively, while a further aero-thermal investigation was performed by Çakan et al. [3, 4], also applying Liquid Crystal Thermometry. More detailed information concerning the aerodynamic behavior of this geometry was obtained by Casarsa and al. [5, 6] using Particle Image Velocimetry (PIV). These investigations clearly put in evidence the complex topology of the flow field, leading to conclude that accurate numerical simulations were necessary to achieve a better understanding of the ongoing processes. Large-Eddy Simulation

Report Documentation Page

Form Approved
OMB No. 0704-0188

1. REPORT DATE	2. REPORT TYPE	3. DATES COVERED
JUN 2007	**N/A**	**-**

4. TITLE AND SUBTITLE	5a. CONTRACT NUMBER
Experimental and Numerical investigation of Flow and Heat Transfer in a Ribbed Square Duct	5b. GRANT NUMBER
	5c. PROGRAM ELEMENT NUMBER
6. AUTHOR(S)	5d. PROJECT NUMBER
	5e. TASK NUMBER
	5f. WORK UNIT NUMBER
7. PERFORMING ORGANIZATION NAME(S) AND ADDRESS(ES) **von Karman Institute for Fluid Dynamics 72 Chaussée de Waterloo B-1640 Rhode-Saint-Genèse, Belgium**	8. PERFORMING ORGANIZATION REPORT NUMBER
9. SPONSORING/MONITORING AGENCY NAME(S) AND ADDRESS(ES)	10. SPONSOR/MONITOR'S ACRONYM(S)
	11. SPONSOR/MONITOR'S REPORT NUMBER(S)

12. DISTRIBUTION/AVAILABILITY STATEMENT
Approved for public release, distribution unlimited

13. SUPPLEMENTARY NOTES
Third International Symposium on Integrating CFD and Experiments in Aerodynamics, June 20-21, 2007, The original document contains color images.

14. ABSTRACT

15. SUBJECT TERMS

16. SECURITY CLASSIFICATION OF:			17. LIMITATION OF ABSTRACT	18. NUMBER OF PAGES	19a. NAME OF RESPONSIBLE PERSON
a. REPORT **unclassified**	b. ABSTRACT **unclassified**	c. THIS PAGE **unclassified**	**UU**	**42**	

Standard Form 298 (Rev. 8-98)
Prescribed by ANSI Std Z39-18

(LES) was therefore applied to the simulation of this flow field to satisfy these requirements. The present approach was validated by Lohász et al. [7, 8] against the aforementioned PIV measurements and applied to the analysis of the flow topology and the role of coherent and persistent structures [9]. The conjugate heat transfer between the flow field and the wall and within the wall of the cooling channel was firstly studied by means of an experimental-numerical investigation. Agostini and Arts [10], applied Infrared Thermography to measure the temperature field on the ribbed surface of the duct and the heat flux was then computed from a conventional conduction code. A first numerical simulation of entire coupled problem by means of LES was presented by Vass and al. [11].

This study can be considered a text-book case of the synergy between experiments and numerical simulations. Experiments have pointed out the existence a complex phenomenology; the simulations (once validated against the measurements) have been applied to help in the interpretation, to gain a more solid understanding of these complicated flow fields and, finally, to identify possible fields of further investigations.

Experimental facility

The experimental part of this investigation was centered on a dedicated facility (Figure 1) designed and built at the VKI. This facility was used mainly for the aerodynamic field determination.

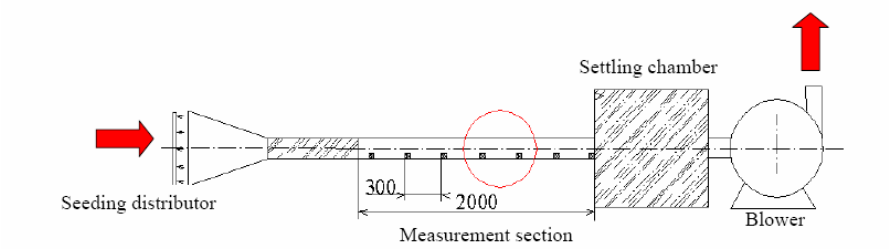

Figure 1: Experimental setup

The test section models a straight cooling channel of a stationary high pressure turbine blade. A good optical access to apply the PIV technique and a high spatial resolution were two major requirements for this investigation. The channel was characterized by a square cross section (100 × 100 mm) and a length of 2800 mm. The measurement section was made of 6 mm thick glass walls while the entrance section was made of wood. Seven ribs were installed on one wall of the channel. The rib cross section was 30 × 30 mm, providing a blockage ratio of 30 %; the ribs were inclined at 90 deg. to the channel axis direction. The rib pitch-to-height ratio (l/h) was equal to 10 and all the measurements were performed between the 4^{th} and the 5^{th} rib, where, as reported in the literature and experimentally checked by Çakan [3] comparing results on successive rib spacings, a mean periodicity was reached in flow and heat transfer characteristics. Moreover, the 5^{th} rib could be replaced by a transparent one for the near wall measurements along two transversal planes. To allow optical access in these regions, a mirror inclined at 45 deg was mounted inside this rib, made of glass.

Air at atmospheric pressure and temperature was ducted through the test section by means of a centrifugal blower. The flow rate was quantified and controlled by measuring the inlet velocity profile and the wall static pressure. The channel was operated at a Reynolds number (based on hydraulic diameter and bulk velocity) equal to $4 \cdot 10^4$, in order to correctly simulate the flow existing in a real cooling channel.

Experimental investigation of the flow field

A two-dimensional PIV technique was used to quantify the flow field characteristics. The measurement chain was made of a two cavities BMI laser, a PCO digital camera with a resolution of 1024 pixels × 1280 pixels and the related acquisition system. The camera and the laser were synchronized at 4.1 Hz by means of a Stanford signal generator. The seeding was provided by oil evaporation using a seeding generator developed at the VKI. The particle sizes ranged between 0.5 and 2 μm, therefore well suited for low Mach number flow measurements. More details about the experimental apparatus were described by Casarsa [6].

The coordinates used in this investigation are X (stream-wise), Y (normal to the ribbed wall) and Z (span-wise). The origin is defined as the intersection between the symmetry plane, the plane carrying the ribs and the span-wise plane dividing the rib in 2 equal parts. The PIV measurements were performed in 5 different planes (Figure 2). The first one is the symmetry plane located at Z/h = 0. Two measurement planes were parallel to the rib-roughened wall, at mid rib height Y/h=0.5 and just above the rib Y/h=1.1. Finally, two YZ planes were located just above the rib at X/h = 0 and at X/h=4.3 to measure the secondary flows.

The selection of these measurement planes was partially based on previous LDV results presented by Rau et al. [1] and allowed a very detailed, quasi 3D view of the whole inter-rib flow field.

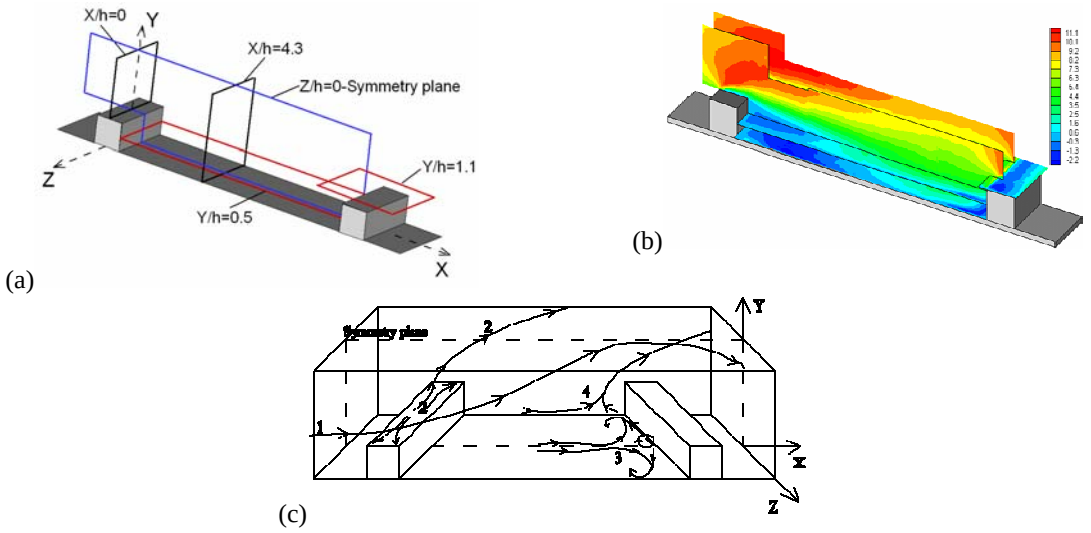

Figure 2: Measurements plane from PIV (a); distribution of stream-wise velocity component (b); topological guess of the flow (c)

All PIV images were processed using W.I.D.I.M., a software developed at the VKI by Scarano et al. [12]. All the data were processed using a 48x48 pixels first interrogation window, one single step of window size refinement and 50% of window overlapping. Two steps of window distortion were used for each step of the refinement procedure. Finally, a Gaussian peak-fitting was adopted to perform the sub-pixel interpolation. With these settings, a minimum of 8820 displacement vectors were defined in each measurement area with a resolution up to 0.03 pixels. Using the Kline and Mc Clintock [13] analysis, the uncertainty on the instantaneous velocity was estimated to be below 2 %.

This experimental campaign has provided a detailed data base. The instantaneous (but unfortunately uncorrelated) character of the PIV measurements allows to look at detailed statistics of the flow field in terms of time mean or time fluctuating quantities. The bulk of these results have been presented by Casarsa et al. [5, 6, 14].

At this point of the discussion it should be clear that the present rib roughened channel flow is characterized by a number of structures, mostly visible in the mean flow field. All these features contribute to the existence of a complicated 3D flow structure covering the whole inter-rib space. Based on the present PIV flow field measurements, supported by previous wall static pressure and LDV measurements, the following mean flow model can be suggested.

Downstream of the reattachment, the flow moves towards the next obstacle and is deviated towards the lateral wall by the pressure-driven transverse flow motion (line 3 in Figure 2 (c)). Then, near the lateral wall, the flow is entrained by a spiral structure (lateral wall/rib corner), but at the same time, is convected upward by the secondary flow (line 4 in Figure 2(c)). The same mechanism takes place upstream of the reattachment, although with a weaker character. On top of the rib, the flow entrained in the separation bubble first moves towards the lateral wall and then is convected upwards by the interaction with the secondary flow (line 2 in Figure 2 (c)). Finally, all the flow that has been displaced to the lateral walls, is then re-convected towards the channel centre thanks to the secondary flow vortex cells (line 1 in Figure 2 (c)). One can therefore conclude that, from a time averaged point of view, the main contribution to the flow renewal on the channel walls, and hence to the augmented heat transfer performance, comes from the secondary flows and the transverse flow motion on the ribbed surface. Their combined effect is indeed to bring the hot flow entrained in the lower layers between the ribs towards the lateral walls and then into the free stream, replacing it with cold flow from the main stream. It is important to keep in mind that the description above is based on a time averaged flow situation.

It must be then remarked that this conceptual model was obtained from a limited number of measurement planes. Moreover, the time series obtained from the PIV measurements were uncorrelated, because of the too low image sampling frequency. Without jeopardizing the experimental approach, a numerical simulation, if correctly validated, could complement the results obtained so far.

Simulation of the flow field over a single rib

Following the conclusions drawn from the experiments it was therefore decided to complement them by three-dimensional simulations in order to provide additional information eventually not accessible by the experiments and to put in evidence the underlying structures driving the process.

Modeling of the turbulence

The key of any simulation of flows at high Reynolds number is obviously the choice of the suitable turbulence model. In the present case, the LES approach has been chosen because it was expected to yield a better performance than RANS in the simulation of complex flows, even in the case approximate wall conditions were applied [15]. This trend was confirmed, among others, by the present authors [7, 8] for the geometry considered in this paper. It must be remarked that LES, besides yielding a better estimation of the Eulerian statistics, is the only tool capable of investigating the unsteady field and, in particular, to put in evidence the presence of vortex structures [16] in the flow and their potential role in heat transfer. The LES capabilities of the commercial finite volume solver FLUENT were applied in the present case.

As well known, the basic idea of the LES turbulence modeling approach is to directly resolve the large scale motions by the solver, while the small (sub-grid) scales are modeled. The two fields are separated through the application of a filter operation on the Navier-Stokes equations. In the case of Finite Differences or Finite Volumes, this filtering operation is implicitly performed by the grid itself and the characteristic length of the filter is related to the cell size Δ. Applied to the Navier-Stokes equations, this operator provides a filtered set of transport equations for the resolved (i.e. “large”) scales:

$$\begin{cases} \overline{u_{j,j}} = 0 \\ \overline{u_{i,t}} + \left(\overline{u_i}\ \overline{u_j}\right)_{,j} = -\rho^{-1}\overline{p_{,i}} + \upsilon\ \overline{u_{i,jj}} - \tau_{ij,j} + \overline{f_i} \end{cases}$$

where the over bar stands for the resolved (filtered) quantities. The vector $\overline{f_i}$ is the forcing term introduced to maintain a constant overall flow rate while applying periodical conditions in the stream-wise direction. The matrix (τ_{ij}) represents the contribution of the small (modeled) scales to the behavior of the resolved field. This term is usually named as "sub-grid stress tensor" (SGS) and is the reduced form of the relationship:

$$\tau_{ij} = \overline{u_i u_j} - \overline{u_i}\ \overline{u_j}$$

Actually, only the deviator part of the SGS stress tensor (τ_{ij}^D) must be modelled, while the isotropic part of the tensor is added to the pressure term, resulting in a "modified pressure". The simplest and most common approach to the modelling of the deviator part of the SGS stress tensor is to introduce the turbulent viscosity concept (υ_T), which leads to the form:

$$\tau_{ij}^D = -2\upsilon_T \overline{S}_{ij}$$

where ($\overline{S}_{ij}$) is the strain tensor written for the resolved scales: $\overline{S}_{ij} = 0.5\ \left(\overline{u}_{i,j} + \overline{u}_{j,i}\right)$.

An equivalent modelling can be applied for the transport of any passive scalar T (the temperature in the present case) yielding:

$$\overline{T}_{,t} + \left(\overline{u}_j \overline{T}\right)_{,j} = \frac{\upsilon}{Pr}\overline{T}_{,jj} - \varphi_{j,j}$$

$$\varphi_j = \overline{Tu_j} - \overline{T}\overline{u}_j = \frac{-\upsilon_T}{Pr_T}\overline{T}_{,j}$$

where (Pr) is the Prantdl number and (Pr_T) is a "sub-grid" turbulent Prantdl number. A detailed description of the technique is provided in [17, 18].

An alternative to the classical LES was proposed in [19], considering the implicit dissipative effect of a high-order upwind scheme with a proper monotone integration of the fluxes. These authors proved that the concept of monotonically integrated LES (MILES) is equivalent to an explicit SGS model. This formulation is suited for Fluent, when a 2nd order limited upwind discretization is used, as done in the present research [7, 8, 9].

Computational field and grid

As previously stated, the measurements were performed in the region where a mean periodicity was reached in flow and heat transfer characteristics. Therefore, it was considered legitimate performing the simulation over a single rib and applying periodic condition along the stream-wise direction. The computational field was made of a single rib with a single pitch extension (Figure 3).

Simulations were performed with a grid using only hexahedral cells. The mesh was weakly unstructured in the X-Y planes and structured in the span-wise direction (Figure 3). The near wall region was composed of a structured layer with a thickness of 0.08D. The size of the first inner cell was 0.003D and the cell-to-cell ratio was 1.09 when moving away from the wall. Finally, the wall layer spanned respectively over 8 cells on the lateral sidewalls, 14 cells over the top of the rib and 10 cells above all other walls. In wall units, the typical distance from the wall of the first cell centre was about $y^+ = 5$, based on an instantaneous wall shear velocity, while the grid spacing in the stream-wise (x) and span-wise (z) directions remained within the limit $\Delta x^+, \Delta z^+ \leq 200$

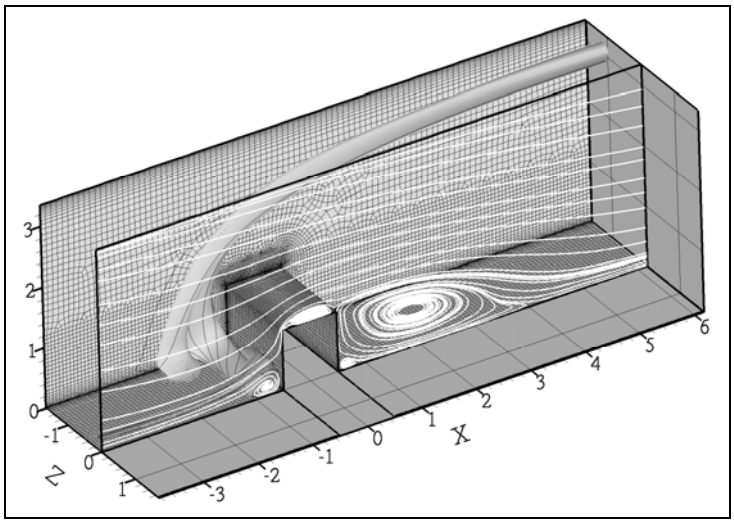

Figure 3: Grid layout on the lateral, bottom and ribbed walls for Z<0 (black lines). Streamlines in the symmetrical plane (white lines). Stream-surfaces illustrating upstream recirculation tube and recirculation tube connecting bottom wall upstream the rib and the top corner of the duct (light grey).

Boundary conditions

The no-slip boundary condition should, obviously, be applied on the walls. On this grid, the cell sizes were incompatible with the LES resolution of the inner wall layer, but were within the range of a correct application of approximate wall conditions [17]. In Fluent, the only wall condition compatible with LES is the standard linear-logarithmic law, applied for velocity and temperature [17]. This situation can be considered acceptable because the grid is sufficiently refined to ensure the first grid point to fall within the linear part of the wall law, ensuring a correct reproduction of the wall gradient. This assumption was validated by the correct reproduction of the pressure drop in the present simulations.

Numerical method and computer execution

The computation was performed using a segregated solver and with a 2nd order bounded upwind differencing scheme for the interpolation of the advection terms and a central scheme for the diffusion terms in the momentum and energy equations. A second order implicit method was invoked for the time discretization.

The simulation was performed using a MILES approach. It has to be noted that a control simulation adding an explicit sub-grid term to the MILES computation had also been implemented. This term was modeled by the well known Smagorinsky model [17] where the turbulent viscosity was:

$$\upsilon_T = L_S^2 \overline{S}$$
$$L_S = min\left(\kappa \ d, C_S V^{1/3} \right)$$

where κ is the von Kármán constant assumed in this work to be equal to 0.42, d is the distance from the nearest wall, V indicates the cell volume and C_s is the Smagorinsky coefficient. This simulation was performed with a value of C_s equal to 0.1. In the following, the nomenclature $C_s = 0.0$ is used to distinguish the MILES results from the one where the MILES computation is complemented with an additional explicit SGS model labelled as $C_s = 0.1$.

The simulations were performed with a time-step of 0.0127 expressed in dimensionless units, based on the characteristic time U/h. This value corresponds to an average value of 0.3 for the fluid Courant number which was found to not exceed the value of 3 anywhere in the duct, in order to avoid a local relaminarization of the flow [20].

First and second order statistics were obtained with an ensemble average of the individual realizations at successive time steps.

Assuming the notation for the ensemble average being $(\langle\ \rangle)$ the fluctuations associated with a resolved quantity are:

$$\bar{f}' = \bar{f} - \langle \bar{f} \rangle$$

The cross component statistics of the resolved stress tensor $\langle \bar{u}_i' \bar{u}_j' \rangle$ were computed as follow:

$$\langle \bar{u}_i' \bar{u}_j' \rangle = \langle \bar{u}_i\, \bar{u}_j \rangle - \langle \bar{u}_i \rangle \langle \bar{u}_j \rangle$$

assuming the number of samples was high enough in the ensemble average. The averaging time of the present simulations was at least equal to 47 times the time necessary for the flow to pass through the complete duct (141 D_H/U_b).

Eulerian statistics

The present approach was validated by comparing its results with the corresponding experimental data for macroscopic engineering parameters and with Eulerian statistics for the average and turbulent fields [7, 8, 9].

From an engineering viewpoint, the averaged pressure drop over one rib-pitch is one of the most important integral parameters characterizing the performance of the ribbed duct. This pressure drop is linked to the friction factor by the following relation:

$$f = \frac{D_H\ \Delta P}{2\, l\, \rho\, U_b^2}$$

In the present case its time averaged value is compared with the one from the companion experiment [5, 6]. The relative importance of the obstruction can be assessed by comparing the friction factor with the one associated to the flow in a smooth pipe of identical hydraulic diameter and Reynolds number. In this last case the Blasius correlation may be used:

$$f_0 = 0.046\ \mathrm{Re}^{-0.2}$$

The experimental and numerical values of the ratio f / f_0 are summarized in Table 1.

	f/f_0
From measurements	12.3±0.25
Simulation with C_s=0	11.636
Simulation with C_s=0.1	12.147

Table 1: Comparison of the friction factor ratios.

The agreement found between the measured value and the one extracted from the CFD computations is rather encouraging. The mismatch observed between the two types of simulations is a first indication that the MILES results are still sensible to the addition of an explicit SGS model. This would confirm that MILES might be sometimes insufficient to totally take into account the interchange between resolved and subgrid scales [21]

The ribbed duct geometry with high blockage is a good example of massively separated flow. Furthermore, inside of a square duct, the sidewalls cause the flow field to be strongly three-dimensional as it can be clearly seen in Figure 3, where four main regions where the flow exhibits a strong rotating nature are easily recognized. The biggest one

(labeled V0 hereafter) represents the main time averaged separation and is located downstream of the rib. The shape and the size of this region are driven by the dynamics of the flow above the rib. The other regions are labeled V1, V2 and V3 and are identified when moving upstream from V0 (see Figure 3). These smaller structures are located respectively in the downstream corner formed by the ribbed wall and the lee side of the rib (V1), attached to the top of the rib (V2) and in the upwind corner formed by the ribbed wall and the wind side of the rib (V3). The associated lengths of these structures in the stream-wise direction are respectively: L_{V0}, L_{V1}, L_{V2} & L_{V3}. The corresponding values are compared with the ones from the companion experimental study [5, 6].

	L_{V0}	L_{V1}	L_{V2}	L_{V3}
Simulation with C_s=0	3.34 h	0.52 h	0.91 h	1.62 h
Simulation with C_s=0.1	3.45 h	0.5 h	0.91 h	2.14 h
PIV experiments	3.76 h - 3.84 h	0.255 h - 0.28 h	0.6 h – 0.9 h	1.04 h - 1.5 h

Table 2: Sizes of the separated regions in the symmetry plane

This comparison is not fully satisfactory for the numerical results. Except for the under predicted size of the largest recirculation area (L_{V0}), all the others sizes are over predicted. Taking the first recirculation upstream (V3), one may notice that the detachment from the wall is produced earlier in the numerical simulation, leading to a higher value of L_{V3}. On the contrary, for the region (V2) located on the top of the rib, the reattachment of the flow on the wall predicted by the numerical results appears latter than the one deduced from PIV, leading to an overestimation of the bubble length. It is believed that the differences noticed on the top of the rib may affect the development of the large recirculation region located downstream to the rib. The size of this last region exhibits a mismatch between MILES and PIV of about 15%, considered acceptable compared to the differences associated with the upstream region. Nevertheless, a PIV campaign zooming on top rib area is currently considered. The length of the secondary structure (V1) is overestimated by an order similar to V3, suggesting that the wall condition is not adequate for these regions.

The averages for the mean velocity and the resolved turbulence are available in [7, 8] and cannot be reported here for space reasons. The overall quality of the present simulations can be assessed from Figure 4. This figure presents the profiles of the mean velocity for the in-plane components of the symmetry plane and of the half rib height plane. It may be seen that except for some small differences in the stream-wise component, the overall agreement is satisfactory. As a preliminary conclusion, the reproduction of the global structure of the flow seems adequate to allow the present authors to consider that the methodology is validated. Furthermore, the acquired database is adequate to be further used in order to reveal the topology of the flow.

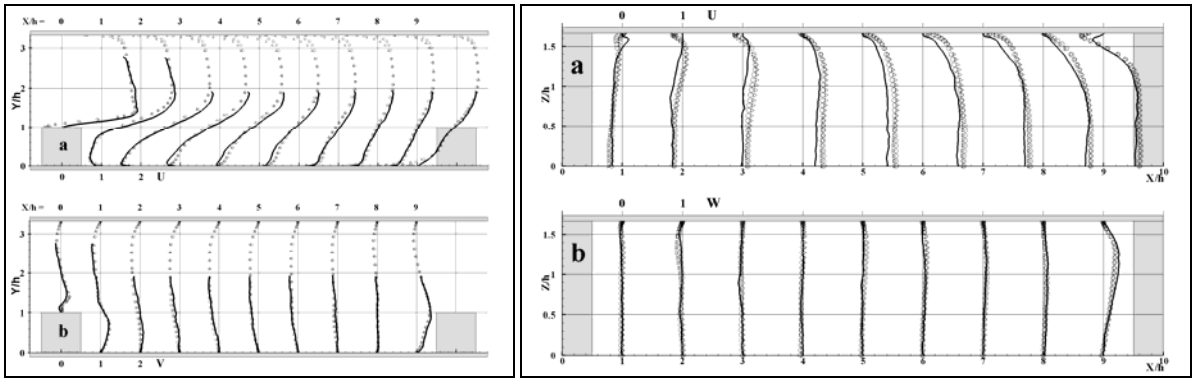

Figure 4: Comparison between simulations (circles (C_s=0); squares (C_s=0.1) and PIV [8] (solid line). Left: In the symmetry plane (Z/h=0) a) X velocity, b) Y velocity. Right: At half rib height (Y/h=0.5), a) X velocity, b) Z velocity. [9]

Topology of the averaged flow

The general phenomenology of the flow above a ribbed surface characterized by a high pitch and at high Reynolds number is illustrated in Figure 3. The interested reader should refer to Cui et al. [22] for complementary aspects on this configuration. Considering that the recirculation regions have been commented in the previous paragraph, it must be noted that although the mean flow in the symmetrical plane may be found similar to the one of a 2D situation, outside the symmetrical plane, the effect of the side and upper walls is strongly felt and the flow becomes completely 3D. In Figure 3, it may be already guessed that the flow in the corner upstream of the rib (location of V3) has a high span-wise velocity component. In the figure, this component is visualized by spiralling streamlines marked on a stream-surface forming a tube trapped in the upstream corner of the rib (this stream-surface is going through the line X/h=-1.08, Y/h=0.05). The pattern of the wall streamlines (Figure 5) shows that this tube escapes upward in the stream-wise direction and is maintained in the low momentum area formed by the sidewall boundary layer, while its 'trace' on the sidewall is materialized by bent wall streamlines. This result confirms the preliminary conclusions drawn from the experiments [1, 2, 3, 4 & 5].

Beside these wall streamlines showing a high upward movement in the windward proximity of the wall, Figure 5**Error! Reference source not found.** also displays bifurcation lines (thick black/white lines), defined as borders where the stream-surfaces detach or reattach themselves from/to the walls [23]. As a matter of fact, for a general 3D flow, a wall shear stress component exists aligned in the direction of the bifurcation line, making arbitrary and useless the definition of the separation and reattachment point used for a 2D flow (zero wall shear stress). Unfortunately, the determination of the bifurcation lines is highly sensible to computational noise due to the always-perfectible level of convergence of the averaged solution and may result in the figures as white and/or black points. These series of points have to been seen (when possible) as continuous lines.

As a qualitative scenario concerning the averaged results, one might propose that the blockage induced by the rib forces the flow in front of the rib to swirl laterally in the sidewall tubes prior to be evacuated over the rib in an upward motion. This motion is balanced in the symmetry plane of the duct by a downward motion, resulting from the presence of a couple of stream-wise elongated counter-rotating structures located in the upper part of the duct (Figure 6 (left)). In Figure 6 (right), attention must be focused on the presence of the high span-wise velocity regions due to the previously mentioned blockage effect of the rib.

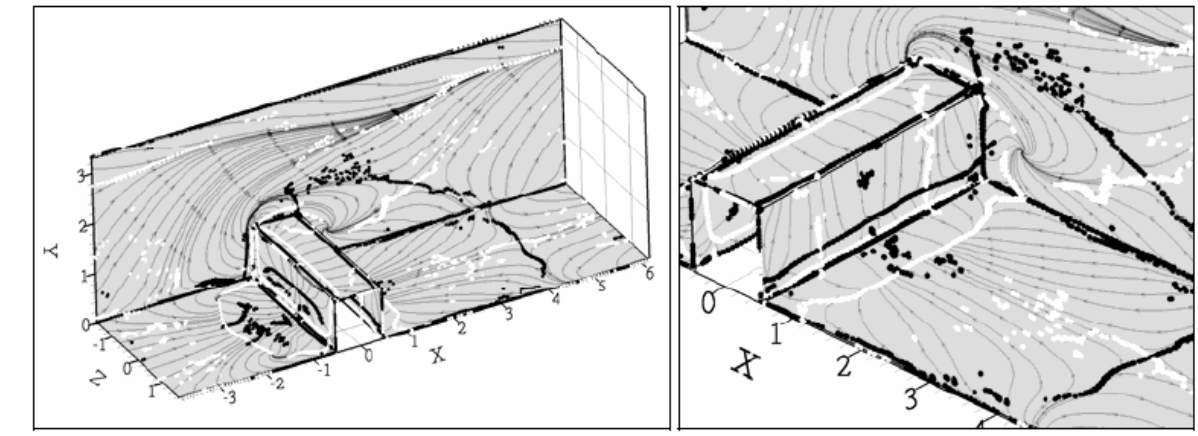

Figure 5: Wall streamlines and bifurcation lines; positive ("separation") black lines, negative ("reattachment") white lines [9].

These results demonstrate that in this geometrical configuration, the sidewalls have a strong influence on the shape of the separated region located on windward side of the rib and they also have an influence, although weaker, on the big recirculation region in the 'wake' of the rib. The swirl away from the wall was already visible through its

footprint on wall streamlines and is confirmed by pattern of the single streamline drawn in the wake of the rib in Figure 6 (right).

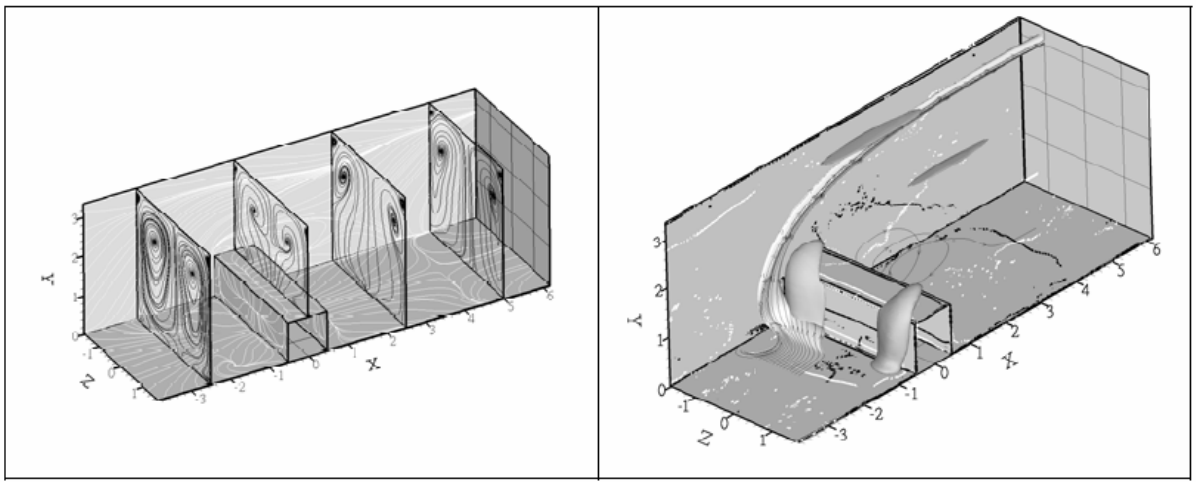

Figure 6: Left) Secondary flow patterns in time-averaged flow (black lines), wall streamlines (white lines). Right) Streamsurface starting from X=-2, Y=0.02 (light grey); Streamline reaching the bottom wall at X=5, Z=-0.3 (black line); isosurfaces of regions of high (0.3 U) spanwise velocity; bifurcation lines. [9]

Another consequence of the upstream separation is the production of a high amount of vorticity. The experimental investigation [4 & 5] advocated that a major part of the vorticity field was induced by the sidewall: the boundary layer on the wall, displaced by the rib, produced extra vorticity in the stream-wise direction. The rotation-dominated vorticity regions can be visualized in instantaneous numerical results by iso-surfaces of the second scalar invariant (Q) of the velocity gradient tensor [24]:

$$Q = \frac{1}{2}\left(\Omega_{ij}\Omega_{ij} - S_{ij}S_{ij}\right)$$

where Ω and S are respectively the anti-symmetrical and the symmetrical part of the velocity gradient tensor. Q is nowadays a commonly accepted and applied criterion to visualize the coherent structures embedded in the instantaneous field [16]). Nevertheless, such a detection tool applied on an averaged field had also been found interesting to investigate rotation dominated regions [15] and it is therefore presented hereafter together with traditional stream surfaces.

For this purpose, the composite Figure 7 (left) presents in the same frame the information given by a Q visualisation, applied on the averaged flow field, and the traditional stream-surfaces. The figure itself is complex to understand because it is composite. On its left part, the stream-surface originating from a line (X/h= -1.08; Y/h=0.05; -1.6<Z/h<0) is displayed. On the other half of the same figure (associated with 0<Z/h<+1.6), the Q iso-surface associated with the value 0.2 U^2/h^2 is shown. Both visualisation techniques underline the structure resulting from the upstream separation in front of the rib, which is lifted up close to the sidewalls by the upward motion previously described and is arched over the rib. One may notice that Q iso-surfaces also highlight the attached recirculation structure on the top of the rib and the duct stream-wise oriented top corner structures. Despite the usefulness of the information yielded by the Q-field, the traditional stream-surfaces remain a powerful tool to put in evidence the high mixing introduced by the rib obstacle. In Figure 7 (right), such surfaces are created by starting a stream-surface from the line (X/h= -3.8; Y/h=0.5; -1.6<Z/h<0) and from the line (X/h= -3.8; Y/h=0.25; 0<Z/h<1.6). It is noticed that the flow belonging to stream surfaces released under Y/h=0.25 is completely lifted up at the side wall.

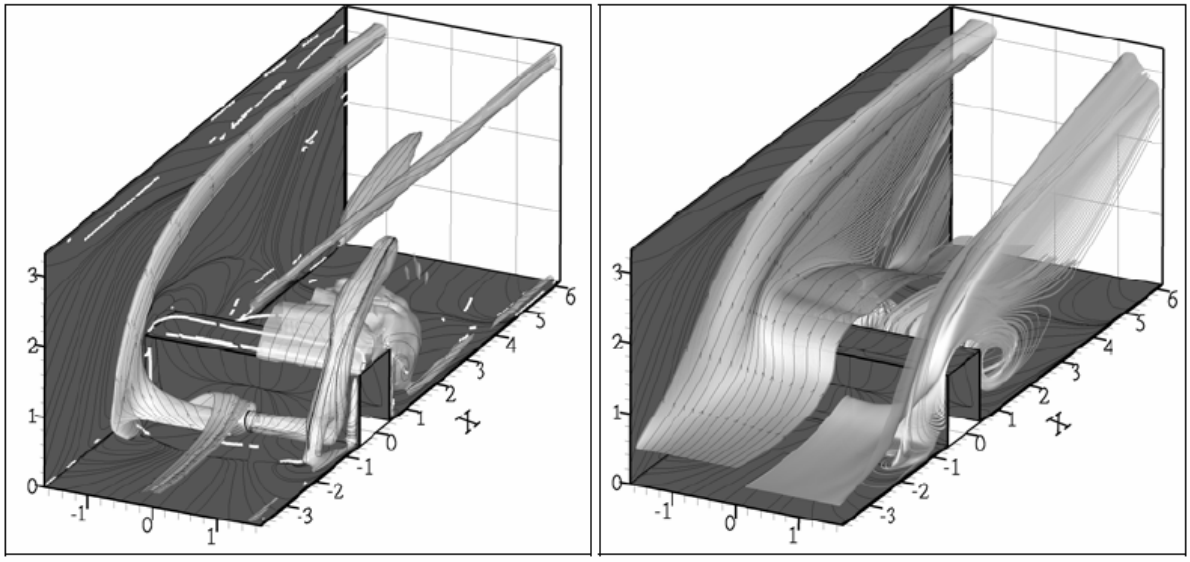

Figure 7: Left) left side (Z<0): streamsurface released from location X=-1.08, Y=0.05; right side (Z>0): Q=0.2 U^2/h^2) isosurfaces; streamlines bounding these isosurfaces (black lines) and wall streamlines (black lines); vortex cores (thick white lines). Right) Streamsurface of time averaged field released from a line at X/h=-3.8, Y/h=0.5 and X/h=-3.8, Y/h=0.25. [9]

A part of this topology was already guessed from the averaged PIV composite fields. The simulation validates the interpretation of the experimental results and clearly points out the fundamental importance of the permanent vortex structures driving the flow.

Simulation of the flow field over three consecutive ribs

Hereafter the simulation performed in order to study the mean and instantaneous coupled heat transfer over three consecutive ribs (Figure 8) is reported. This configuration does not use periodic conditions but "open type" boundary conditions labeled as inlet (for the flow entering the domain) and outlet (for the flow exiting the domain).

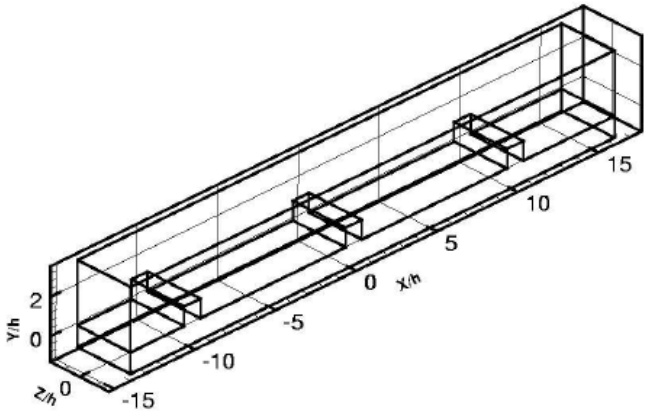

Figure 8: Computational field for 3 consecutive ribs

A study on this configuration was motivated by two main reasons:
- it was considered important to verify, as far as feasible, the assumption that ALL the features of the flow repeat themselves over every pitch length. For this, the potential existence of long scale flow structures extending over more than one pitch had to be investigated. It has to be noted that the time averaged inlet plane was a solution extracted from a periodic simulation.
- From a practical point of view, it was found impossible to extend the present simulation to study the instantaneous heat transfer, because the present solver (FLUENT 6.2) supports periodic boundary conditions for heat transfer in a fluid only by fixing the temperature at a constant value in the cell of index 1. It was then proposed to overcome this limitation by performing simulations over three successive ribs and to take into account the evolution of the thermal field along the stream-wise direction. The initial hypothesis was that, applying a realistic description of the developed flow at the inlet, the computed flow would stabilize itself over the first pitch, the solution over the second pitch would be representative of the full periodic flow and the third pitch would damp the perturbation introduced by the outlet boundary condition. This hypothesis is reflected in the fact that the grid was refined over the second pitch.

Computational field and grid for the simulation of 3 consecutive ribs

The new computational field is made of three consecutive ribs, geometrically identical to the one studied with periodic conditions. As one of the aims of this investigation was to study the coupled heat transfer between the wall of the experimental facility (and ultimately the turbine blade) and the cooling fluid, the fluid of the CFD domain was coupled with a solid slab of stainless steel, made by of the bottom wall supporting the ribs themselves. The thickness of this slab *s* corresponding to $s/h = 1.1$ in the present adimensionalization. Buoyancy and viscous heating effects are neglected in the simulation.

The grid is similar to the one applied in the preceeding part: **t**he structured blocks near the ribbed wall had a thickness of 0.08D with a starting size of 0.002D at the wall and contained 13 cells normal to the wall. The growth rate of the cell size was constant moving away from the wall. At the top wall, the thickness of the structured block was 0.1D and contained 10 cells starting with a size of 0.003D. On the lateral walls the mesh had the same resolution in the boundary layer as on the ribbed walls. As already stated, the grid outside of the boundary layer was more refined around the second pitch, to increase the accuracy of the simulation in the supposed most interesting region.

In the solid part of the computational domain a similar mesh was applied, refined near the wall and inside the rib. The number of cells in the fluid was in excess of 830,000, while the whole computational domain did amount up to 1,170,000 cells.

Boundary Conditions

At the inlet, the boundary condition is made of the averaged velocity plane, obtained from a one-rib steady state RANS computation (periodic conditions were used in the stream-wise direction), and a superposed perturbation to initiate the development of the turbulent fluctuations. For this task, the technique of Smirnov et al. [24] was employed, with parameters based on the RANS turbulence kinetic energy and dissipation profiles. Zero diffusion-flux in the direction normal to the exit plane was applied as outlet boundary condition. Concerning the energy equation, adiabatic boundary conditions were imposed on the top and lateral walls of the channel and on the lateral walls of the slab. On the bottom of the slab a constant heat-flux was fixed at a value of 2220 W/m^2. The ribbed surface of the duct is coupled for heat transfer with the solid.

Eulerian statistics

The first question to be answered is whether the present inlet conditions and computational domain allow the simulated flow to reach the fully developed state downstream of the first pitch length. A first qualitative answer can be extracted from Figure 9 which shows the time-averaged streamlines in the symmetry plane, for the three pitch lengths and for the previous simulation with periodic boundary conditions in the stream-wise direction.

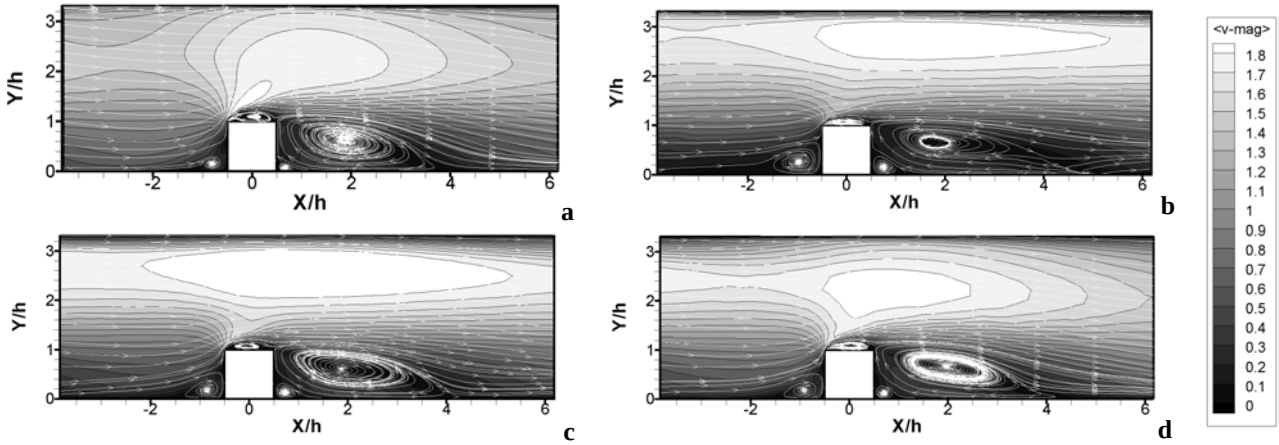

Figure 9: Contours of mean velocity magnitude at Z/h=0 with streamlines in case of periodic bc. [6] (a), and in case of classic inlet-outflow bc. on 1st (b), 2nd (c) and 3rd (d) pitch. [11].

Figure 9 shows the evolution of the flow along the stream-wise direction. Around the first rib, the shape and size of the separated regions are strongly different from the ones in the reference (periodic) case, while the ones for the second and third pitch are closer and comparable. However, the size and shape of the high velocity region above the rib are only reproduced for the third obstacle. This indication is confirmed by the analysis of the Eulerian statistics of the flow [10].

Comparing the pressure drop due to the presence of the ribs it can see that the experimental value is recovered only over the 3rd pitch (see Table 3 to be compared with Table 1).

	f/f0
LES with inlet-outflow bc. (2nd pitch):	8.1
LES with inlet-outflow bc. (3rd pitch):	12.154

Table 3: Comparison of the friction factor ratio for different pitches.

Detailed statistics, namely the profiles of stream-wise and vertical mean velocity components, the variance of the stream-wise velocity component and the covariance of the two velocity components are shown in Figure 10: profiles of mean stream-wise (a) and vertical (b) velocity components, variance of stream-wise (c) and covariance of stream-wise and vertical (d) components. They confirm that the present simulated flow is close to the periodic LES and the PIV results only across the third pitch length. Above the second rib, the mean stream-wise velocity is overestimated in high velocity regions and under-predicted in low velocity areas. The mean velocity vertical component is underestimated all over the second pitch. The calculated mean velocity components show a rather good agreement with the measurements. Across the third pitch, the profiles of the stream-wise velocity variance match well with the experimental results, although peak values are slightly lower for the LES predictions. The covariance peaks for the stream-wise and vertical velocity components are under-predicted in the planes on the downstream side of the rib while on top and in front of the rib the measurements agree well with the simulation.

These results lead to the conclusion that the present mesh and inlet condition do not seem fully adequate to allow the flow to establish itself over one rib pitch. Only the flow over the third rib matches well the reference.

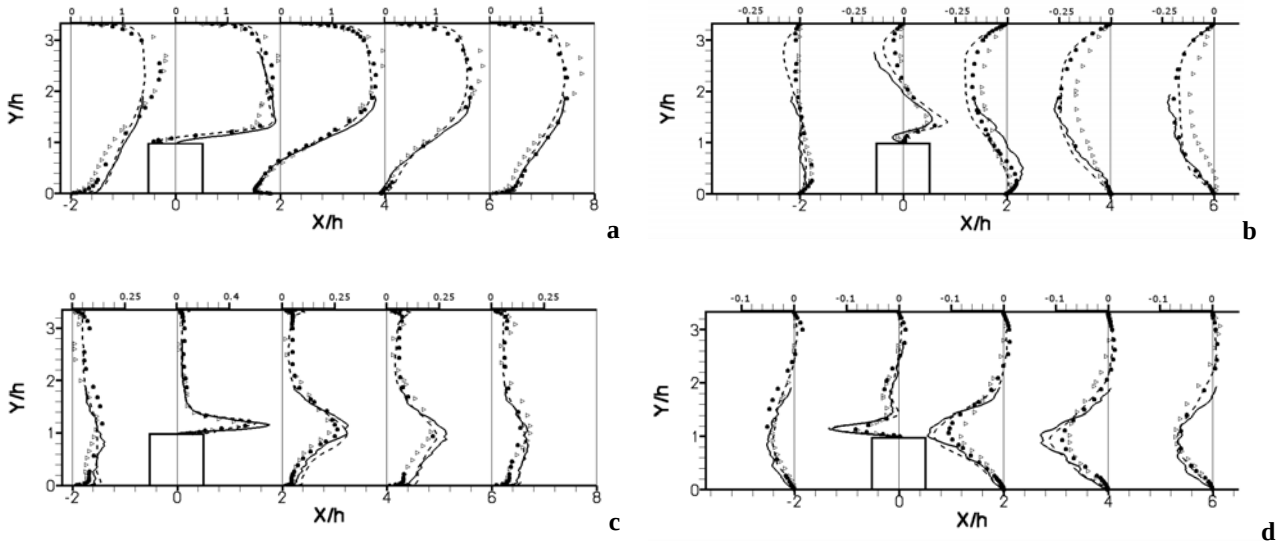

Figure 10: Profiles of mean stream-wise (a) and vertical (b) velocity components, variance of stream-wise (c) and covariance of stream-wise and vertical (d) components. Symbols denote: PIV - continuous line; LES with periodic bc. – dashed line; LES with extended domain: 2nd pitch – right triangle; 3rd pitch – dot. [11]

Over this pitch, the results are satisfactory despite the coarser grid and the proximity of the "Outlet" boundary condition. The present flow field is therefore adequate to study the heat transfer in this configuration.

Topology of the average flow field

The presence and the role of permanent structures in this flow were already put in evidence in previous LES simulations; the new results offer new indications and perspectives.

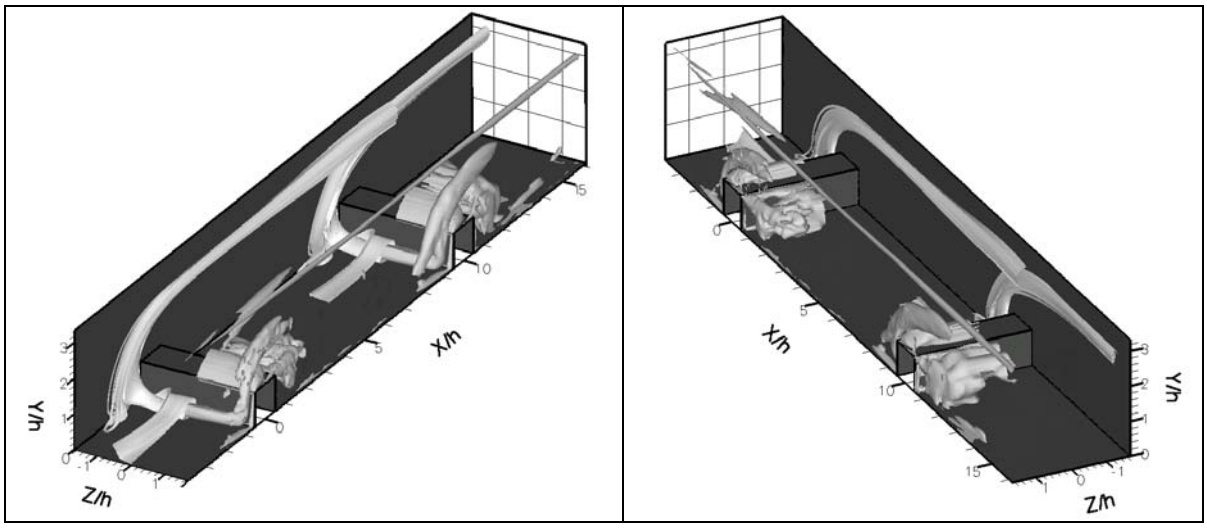

Figure 11: Stream-traces (Z negative) and coherent structures extracted from the mean flow (Z positive) across the second and third rib [10]

For this purpose, the composite Figure 11 presents two views, showing, for the averaged flow field, the Q iso-surface associated with the value 0.45 U^2/h^2 and the stream surface issued from a line (X/h= -1.08; Y/h=0.05; -1.6<Z/h<0). Both representations underline the importance of the structure resulting from the upstream separation on the ribbed wall, which is lifted up close to the sidewall by the upward motion visible in Figure 11, and which arches over the rib. An information of potential importance is the presence of structures larger than one pitch length, which could indicate that the study (experimental or numerical) might be insufficient for a complete understanding of the present flow.

Investigation of heat transfer

The conclusions drawn in the previous paragraph allow evaluating the heat transfer results extracted from the present simulation. The "sub-grid" turbulent Prantdl number was fixed at 0.85 for the present simulation. An overall view of the results is presented in Figure 12, which shows the average temperature of the entire computational field for the symmetry plane.

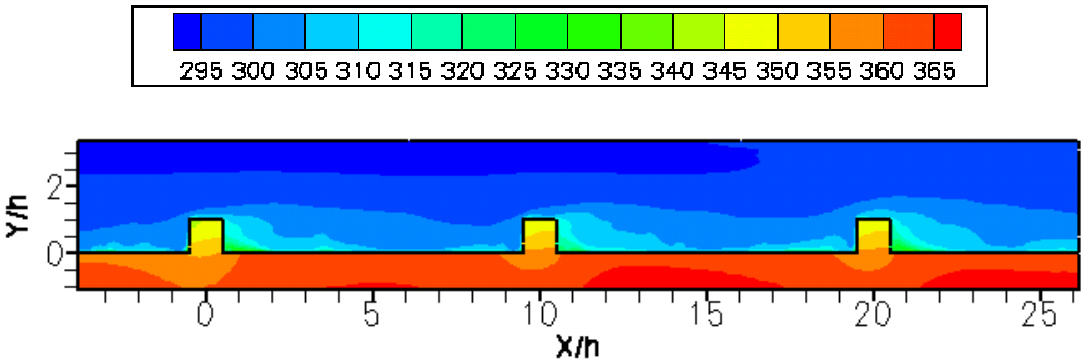

Figure 12: Average temperatures in the symmetry plane in K^o (Z=0)

The strong effect of the rib on the heat transfer is obvious, while the similarity of the temperature field around the second and the third rib allows concluding that the results for the last rib can be considered representative of the fully established situation.

In engineering terms, the effect of the rib on heat transfer is assessed through the Enhancement Factor (EF), which represents the ratio of the local Nusselt number along the present duct:

$$Nu = f(\mathrm{Re}, \mathrm{Pr}) = \frac{h(x;y)D_h}{k_{air}}$$

and along a smooth one, operated at the same Reynolds number:

$$Nu_0 = 0.023\mathrm{Re}^{0.8}\,\mathrm{Pr}^{0.4}$$

$$EF = \frac{Nu(x,y)}{Nu_0} = \frac{\dot{q}D_h}{0.023\,\mathrm{Re}^{0.8}\,\mathrm{Pr}^{0.4}(T_w - T_b)k_{air}}$$

Figure 13 presents the distribution of EF along the symmetry line, for the present simulation and the experimental data obtained applying, respectively, liquid crystal thermometry and IR thermography. Based on the previous observations, one would expect an increased heat flux on the upstream surface of the rib, and a pattern following the topology i.e. lower heat transfer at separation and higher at reattachment zones. The numerical results follow this tendency.

Important differences are remarked between the results of the two experimental techniques, but can be explained by the different experiment conditions. The liquid crystal results [3] are obtained for a uniform heat flux thermal boundary condition along the ribbed wall and are unable to catch the strong gradients of heat transfer on the upstream and top faces of the rib. The infra-red data results [10] have been extracted from a conjugate approach and should, therefore, be much closer to the present computation. These experiments show that the majority of the heat is extracted at the top surface of the rib, while the net energy balance at the wind- and leeward side of the rib is around zero. The numerical simulation appears to match fairly well the experiments upstream and downstream of the rib. The agreement on the rib faces is more questionable.

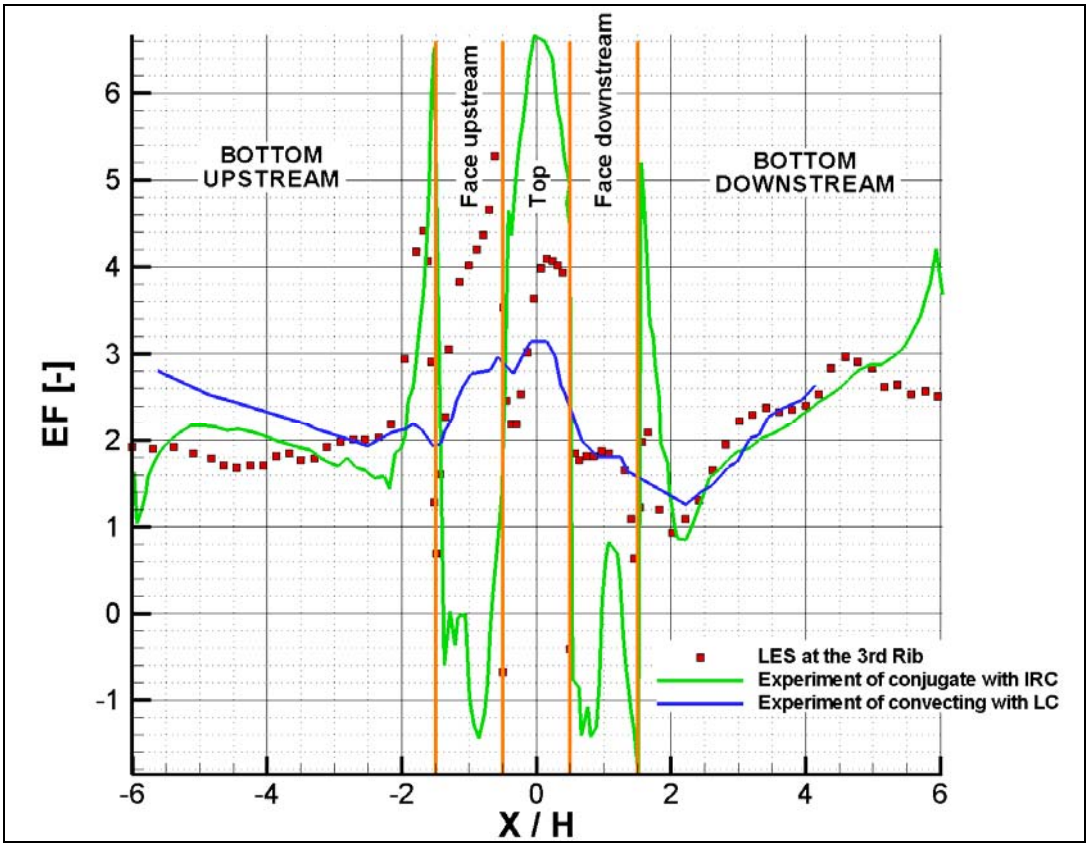

Figure 13: Profiles of enhancement factor along the section of the bottom line and mid-plane. LES: Large eddy simulation IR: Infra Red Camera, LC: Liquid Crystal. [11]

Different explanations could be thought for the differences between the results of the experimental and numerical investigations. The initial field was obtained from a RANS simulation: the k-ε turbulence model applied in the latter seems to be unable to describe accurately the studied phenomenon, failing especially, in simulating turbulence generated secondary flows. As a result, heat transfer is underpredicted between the coolant and the channel wall, which leads to over-predicted wall temperature. A proposed alternative could be the solution of the energy equation using the mean velocity and Reynolds stress fields obtained from LES, therefore having a better estimation for the turbulent thermal conductivity coefficient as well. The available time made it impossible to investigate the effect of the choice of the value of the subgrid Prandtl number, topic to be tackled in future investigations.

Finally, regions of slightly negative EF's (meaning a negative heat flux) are observed in Figure 13 for the experimental measurements and for the simulation. Rigorously, such a negative heat transfer coefficient cannot exist. This result is due to the present definition of EF, based on the mean bulk flow temperature. Consequently, a

local flow temperature higher than the wall temperature would result in a local positive heat transfer coefficient. This situation is possible for the incoming flow just upstream of the rib, which is trapped in a re-circulation bubble. The flow in this bubble presents a low level of mixing and re-circulates near the front surface of the rib, a zone in contact with the bottom wall, which has a relatively high temperature; therefore the fluid can be heated above the temperature of the face of the rib. This would explain the inversion of the sign of the temperature difference between the cold rib front wall and the local flow temperature and justifies the present results. A similar observation can be made for the results along the back wall of the obstacle. The observation of this effect in both numerical and experimental results represents a further of the capability of the simulation to support and validate the experiments and vice versa.

To further investigate this trend, the entire map of EF over the third pitch is presented in Figure 14. It is evident that the negative EFs are located at the corners between rib and bottom wall, which is consistent with the present qualitative interpretation. Outside of these regions, the distribution of the simulated EF shows a consistent trend with the experimental data.

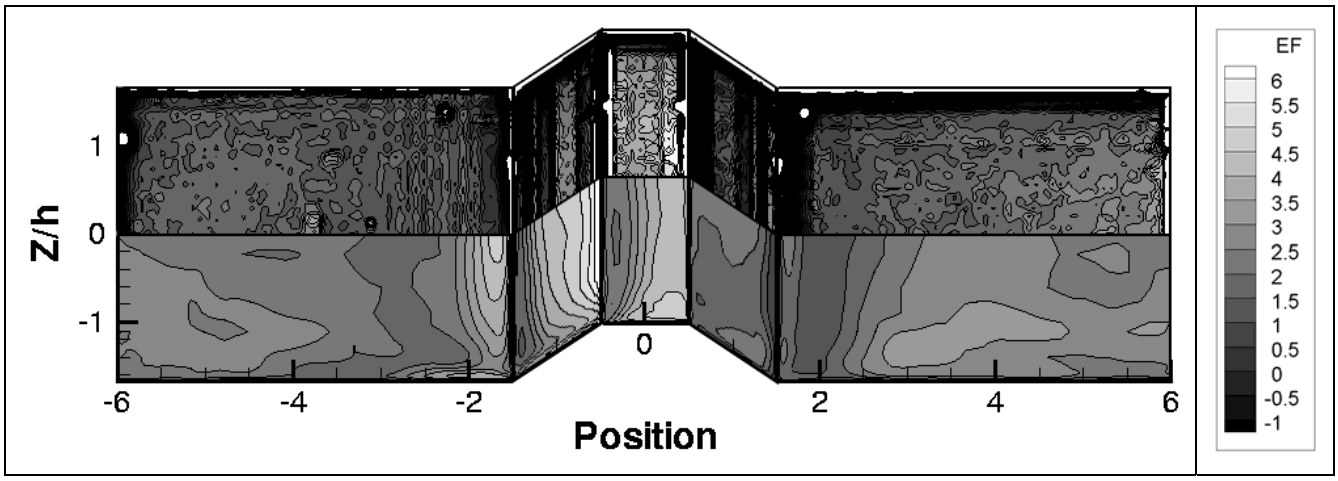

Figure 14: Enhancement factor according to IR thermography (upper) and LES (lower). [11]

Conclusions

The present paper has highlighted the possible interactions between experiments and numerical simulations in the investigation of a complex flow problem. It has shown how the numerical simulations can be used to explain and complete the experimental investigation, validating its findings and interpretation in the light of the information which not accessible by the experiments but readily available by three-dimensional numerical approach. In the case of the ribbed duct, the simulation has put in evidence the underlying structure which drives the processes proposed on the basis of the experimental data. The existence and the importance of permanent vortex structures in the flow have been demonstrated and their role in the topology of the mean flow has been shown.

Further simulations have shown that it is feasible to simulate the flow and heat transfer in a ribbed cooling channel applying “natural” inlet-outlet boundary conditions instead of periodic boundary conditions in the stream-wise direction, even if a much larger computational field is necessary as it was found that the flow reached equilibrium only at the third pitch. A potentially important finding of this investigation is that it has put in evidence the presence

of time averaged structures longer than one pitch, which should be taken in account and investigated for any future study to assess and apply experimental or numerical results obtained on a single pitch.

The validation with heat transfer measurements yielded good results on the ribbed surface, but higher differences on the surface of the rib itself. It must be remarked that the simulation has confirmed the apparently unphysical result of the existence of regions of negative EF which had already been remarked from the experience. This agreement represents a further demonstration of the capability of joint experimental/simulation approaches to complex flow problems.

Acknowledgements

The present paper has summarized the history and the results of the research performed at the von Karman Institute for the understanding of the transport processes in ribbed ducts. Most of these reports have been obtained in the frame of the research programs of the post-graduated students of the von Karman Institute and notably the Ph.D theses of Dr G. Rau, M. Çakan and L. Casarsa, and the ongoing Ph.D research work of Mr. M.M. Lohász and P. Vass.

References

[1] G. Rau; D. Moeller; M. Çakan; T. Arts. (1998). The effect of periodic ribs on the local aerodynamic and heat performance of a straight cooling channel", *J. of Turbomachinery, Vol. 120, pp 368-37*5

[2] G. Rau (1998). Einfluss der Rippenanordnung auf das Strömungsfeld und den Wärmeübergang in einem Kühlkanal mit quadratischem Querschnitt. Ph.D. Thesis, Technischen Universität Darmstadt, Germany.

[3] M. Çakan. (2000). Aero-thermal investigation of fixed rib-roughened internal cooling passages. PhD thesis, Université Catholique de Louvain, Von Karman Institute for Fluid Dynamics

[4] M. Çakan and T. Arts (1997). Effect of rib height on heat transfer enhancement in a cooling channel. *Eurotherm Seminar No 55, Heat Transfer in Single Phase Flows, Santorini, Greece.*

[5] L. Casarsa; M. Çakan; T. Arts. (2002). Characterization of the velocity and heat transfer fields in an internal cooling channel with high blockage ratio. *Proceedings of ASME TURBO EXPO 2002 June 3-6, 2002 Amsterdam, The Netherlands*

[6] L. Casarsa (2003). Aerodynamic performance investigation of a fixed rib-roughened internal cooling passage. PhD Thesis, Universita degli Studi di Udine, Von Karman Institute for Fluid Dynamics

[7] M.M.Lohász ; P. Rambaud; C.Benocci (2003). LES simulation of ribbed square duct flow with Fluent and comparison with PIV data. *Conference on Modeling Fluid Flow CMFF'03 The 12th International Conference on Fluid Flow Technologies, Budapest, Hungary*

[8] M.M.Lohász ; P. Rambaud; C.Benocci (2004). MILES flow inside a square section ribbed duct. RTO *Meeting, AVT-120 Workshop on "Urban Dispersion Modeling" April 1-2., Rhode-Saint-Genèse, Belgium*

[9] M.M.Lohász ; P. Rambaud; C.Benocci (2005). Flow features in a fully developed ribbed duct flow as a result of LES. *Engineering Turbulence Modeling and Experiments 6 – Proceedings of ERCOFTAC ETMM6, 23-25May, Sardinia, Italy, 267-276*

[10] F. Agostini and T. Arts, (2005). Conjugate heat transfer investigation of rib-roughened cooling channels. *Proceedings of ASME Turbo Expo*, June 6-9, Reno-Tahoe, Nevada, USA

[11] P. Vass; P. Rambaud; T. Arts; C. Benocci (2007) Numerical investigation in flow and heat transfer in a ribbed square duct applying LES. *7TH ETC Conference Athenes, 4March; Greece*

[12] F. Scarano (2000), Particle Image Velocimetry, Development and Application. PhD Thesis, Università di Napoli Frederico Secondo, Italy

[13] S.J Kline and F.A.Mc Clintock (1953). Describing Uncertainty in Single-Sample experiments. *Mechanical Engineering, Vol. 75, pp 3-8*

[14] L. Casarsa and T. Arts (2007). Combined heat transfer and flow field analysis in rib-roughened cooling passages for turbine blades. *7TH ETC Conference Athenes, 4March; Greece*

[15] W. Rodi, J.H. Ferziger, M. Breuer and M. Pourquie (1997). Status of Large Eddy Simulation: Results of a Workshop. *J. Fluids Eng.*", 119, 248--262

[16] Y. Dubief, and F. Delcayre. (2000). On coherent-vortex identification in turbulence. *Journal of Turbulence*, **1,** 011

[17] U. Piomelli (2006). Large eddy simulation and related techniques; theory and applications. *Large Eddy Simulation of Turbulent Flows, VKI Lecture Series 2006-04.*

[18] S.B Pope (2000). Chapter 13: Large-eddy simulation. *Turbulent Flows, Cambridge University Press.*

[19] J.P. Boris; F.F. Grinstein; S.S Oran; R.L. Kolbe, (1992). New insight into large eddy simulation. *Fluid dynamics research.* **10.** 199-228.

[20] H. Choi and P. Moin (1994). Effects of the Computational Time Step on Numerical Solutions of Turbulent Flow, *Journal of Computational Physics*, **133,** 1-4.

[21] P. Comte and M.Leiseur (1998) . Large-Eddy Simulations of Compressible Turbulent Flows. L.E.G.I./Institut de mecanique de Grenoble, France. *VKI LS 1998-05, Advances in Turbulence Modelling, March 23-27,*

[22] J. Cui; . V.C.Patel and C.-L Lin (2003). Large-eddy simulation of turbulent flow in a channel with rib roughness. *International Journal of Heat and Fluid Flow,* **24**, 372-388.

[23] H. Hornung,and A. E.Perry, (1984). Some aspect of three dimensional separation Part I.: Streamsurface bifurcations. *Zeitschrift für Flugwissenschaften und Weltraumforschung,* **8,** 77-87.

[24] J. C. R. Hunt; A. A Wray, and P Moin,. (1988). Eddies, Streams, and Convergence Zones in TurbulentFlows. *Center for Turbulence research, Proceedings of the summer Program*

[25] A. Ooi;. B.A Petterson Reif;,. G. Iaccarino and P.A. Durbin, (2002). RANS calculations of secondary flow structures in ribbed ducts. *Center for Turbulence, Research Proceedings of the Summer Program 2002*

[26] A.Smirnov.; S. Shi.; I. Celik (2001). Random flow generation technique for large eddy simulations and particle-dynamics modeling. *Journal of Fluids Engineering,* **123,** 359-371.

Experimental and Numerical investigation of Flow and Heat Transfer in a Ribbed Square Duct.

Tony Arts arts@vki.ac.be
Carlo Benocci benocci@vki.ac.be
Patrick Rambaud rambaud@vki.ac.be

Outline

- Motivations & objectives.
- Experimental setup and preliminary results (PIV).
- Numerical configuration and preliminary results (LES). [1 & 3 ribs]
- Comparison & cross validation.
- Conclusions & future works

Motivations & Objectives

Motivations:

- To Improve Turbine Blades Internal Wall Cooling.

Why:

- Temperature exceeds melting point of blade material (efficient cooling is mandatory to avoid catastrophic failure).

How:

- Heat transfer inside the blade is enhanced by ribs in cooling channels.

Objectives:

- Combine experimental & CFD approaches to better understand the physical phenomena. Experiments alone cannot provide all the answers.

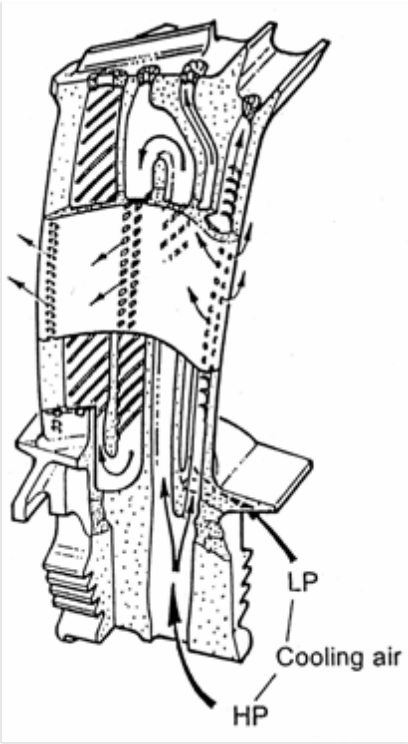

Experimental Setup

Scaled-up models (D_h=100mm) of an internal cooling passage for HP turbine.

- straight channel
- square section, L/D_h=20
- one ribbed wall
- square ribs, α=90°, p/h=10, h/D_h=0.3

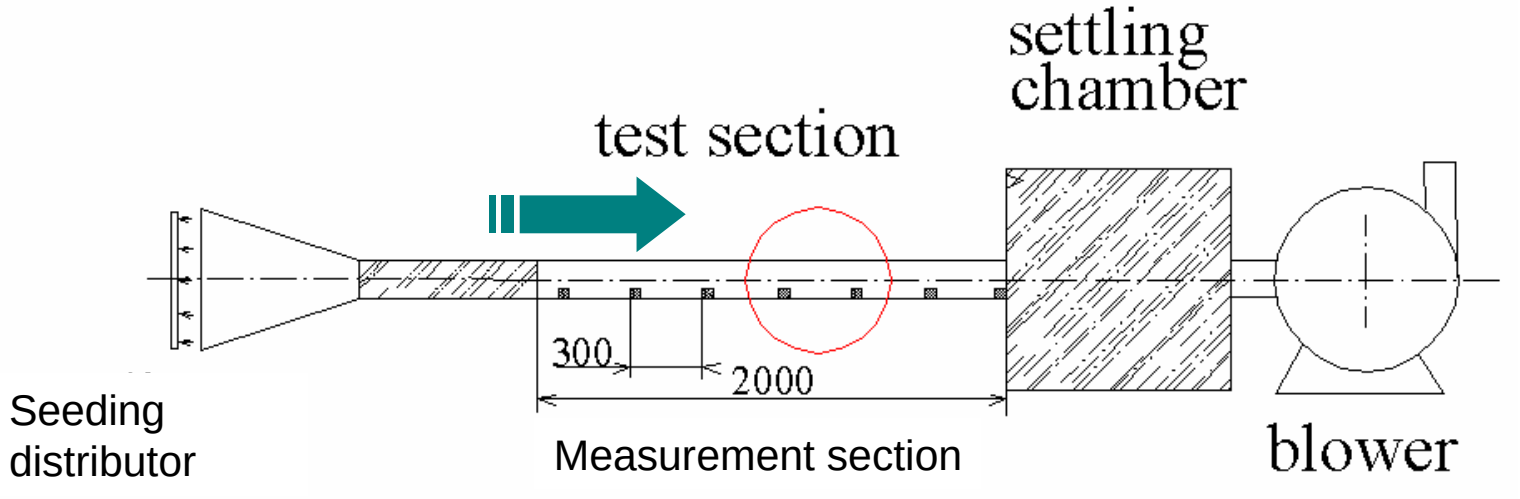

Measurement performed in between the 4th and the 5th rib

$$\mathrm{Re} = \frac{\rho U_0 D_h}{\mu} \approx 40000$$

Experimental Techniques

Dynamic of the flow: Particle Image Velocimetry

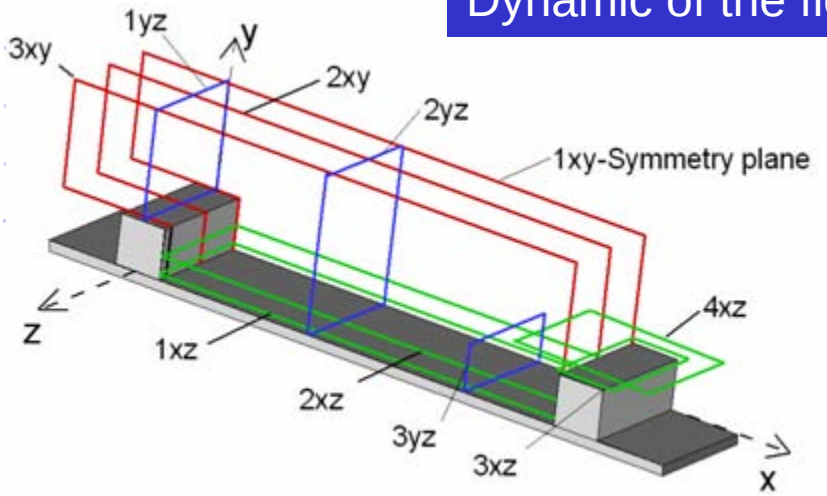

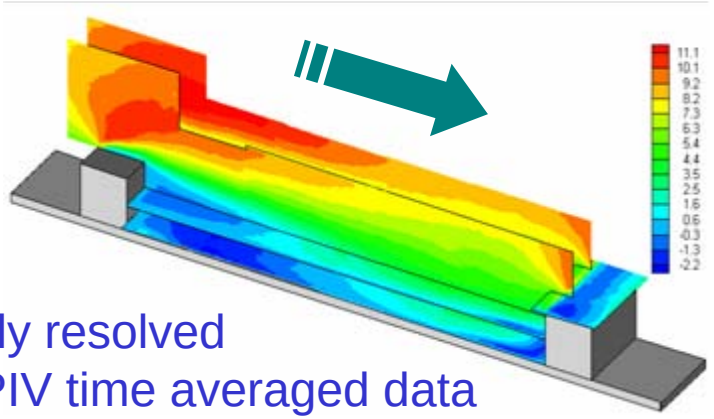

Highly resolved
2D-PIV time averaged data

Thermograph of the interface solid/gas: Infrared Camera

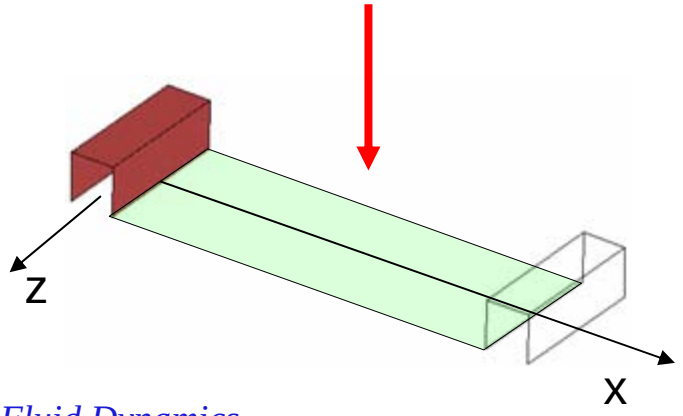

PIV Results

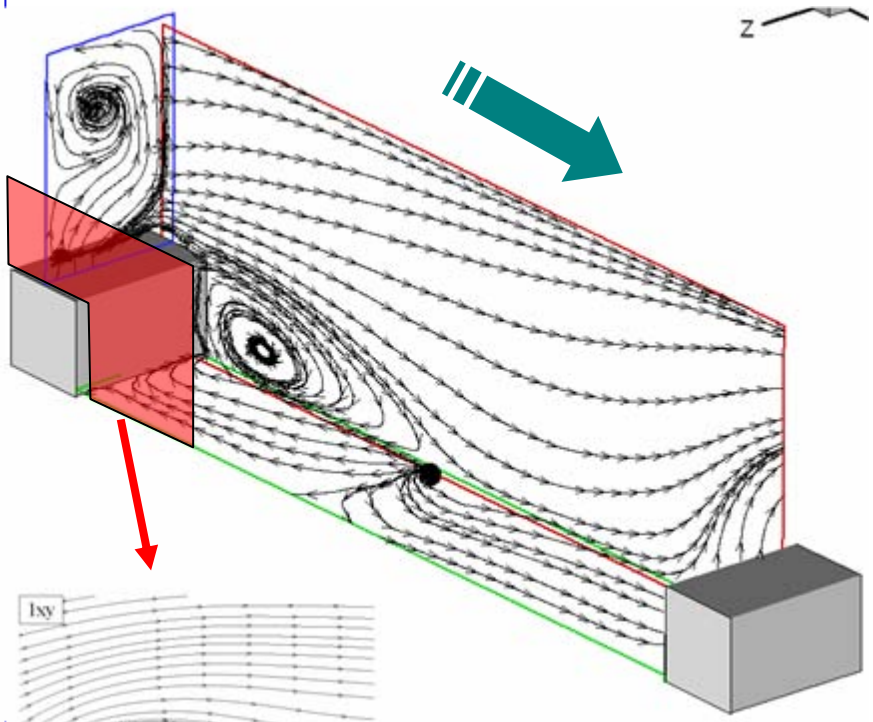

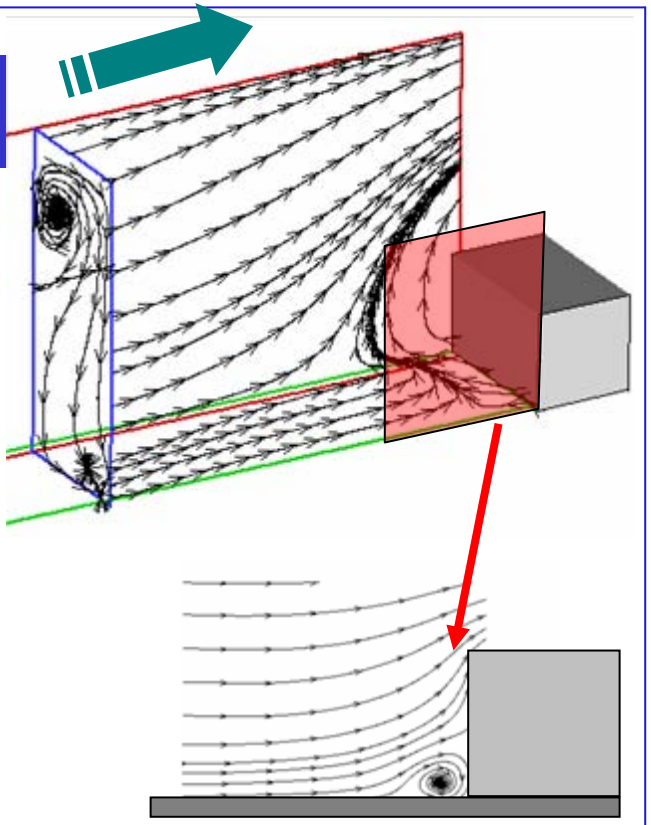

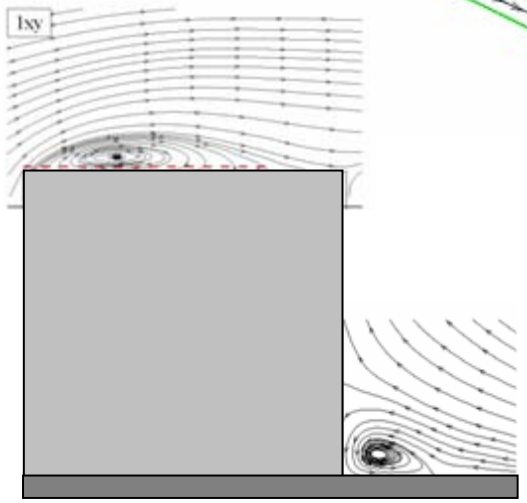

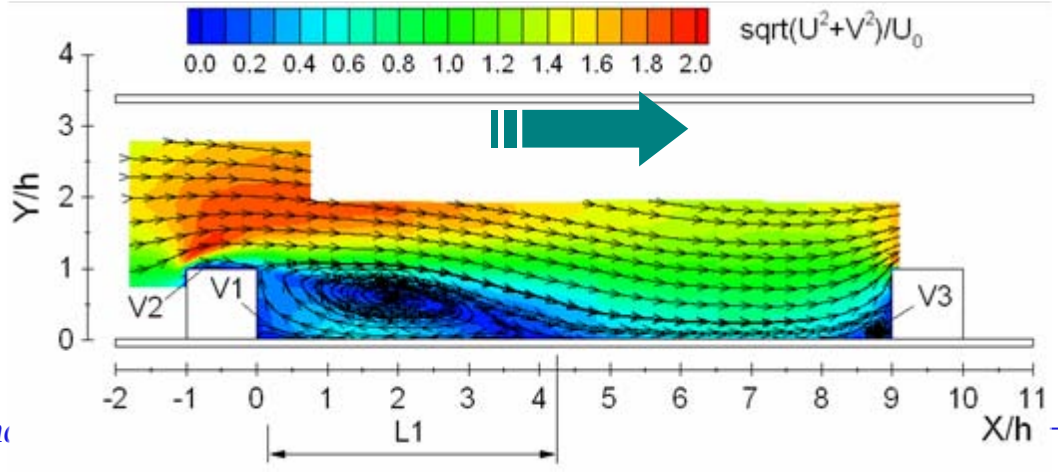

Experimental Results

Topology of the time averaged flow is guessed (interpretation).

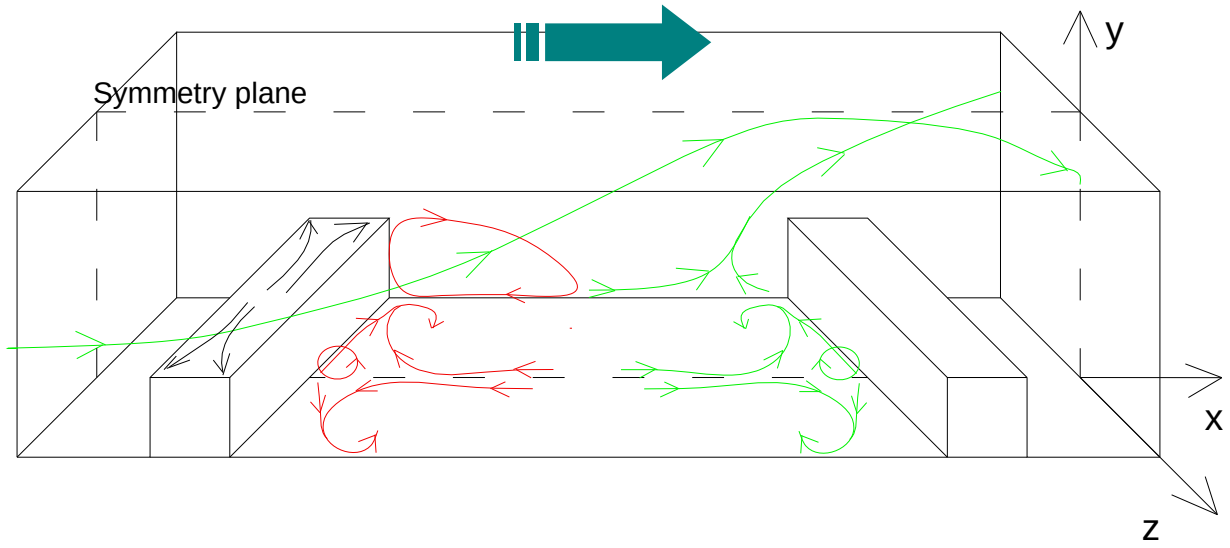

This topology will be confirmed but also slightly corrected thanks to CFD.

Possible CFD strategies

- Geometries: Engine-like ⟷ Simplified
- Configuration: Rotating ⟷ Non-Rotating
- Heat BC: Temperature/flux at interface wall ⟷ Conjugate heat transfer
- Turbulence: RANS, URANS ⟷ LES

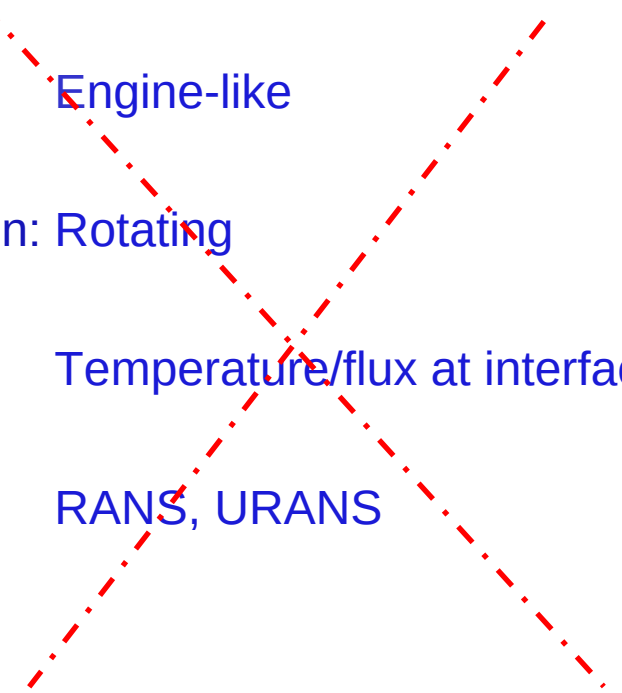

Simplified method & the conjugate method

- CFD done with the commercial code FLUENT [v6.2.16]
- Only 1 rib using period boundary conditions
- Computation of the temperature field in the fluid and the solid simultaneously
- Coupling of heat-transfer through the top surface of the solid part
- Applying uniform, constant heat-flux on the bottom of the slab

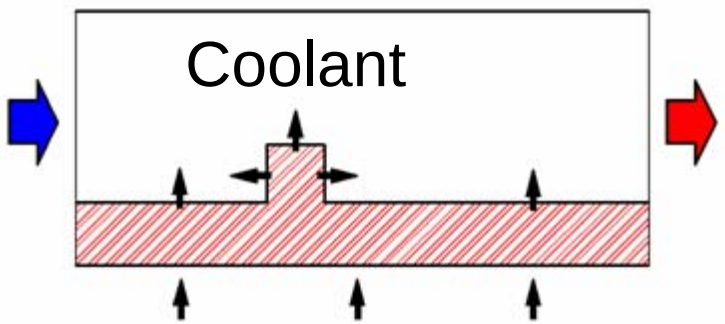

Dynamic over a single rib

Good validation of the topology guessed from PIV with some corrections in the wake of the rib.

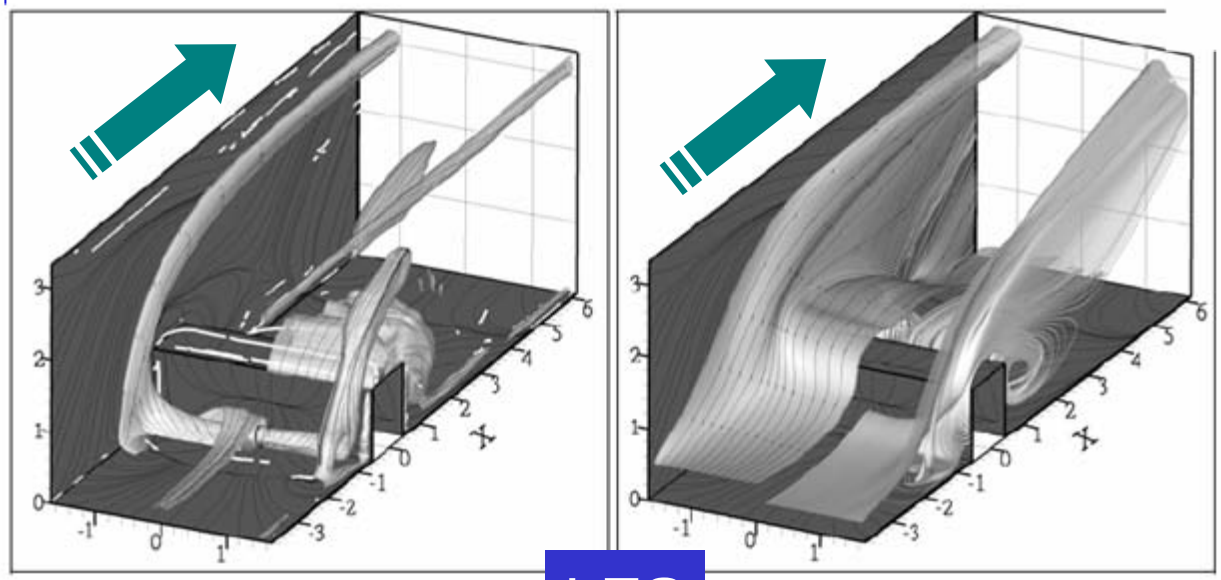

LES

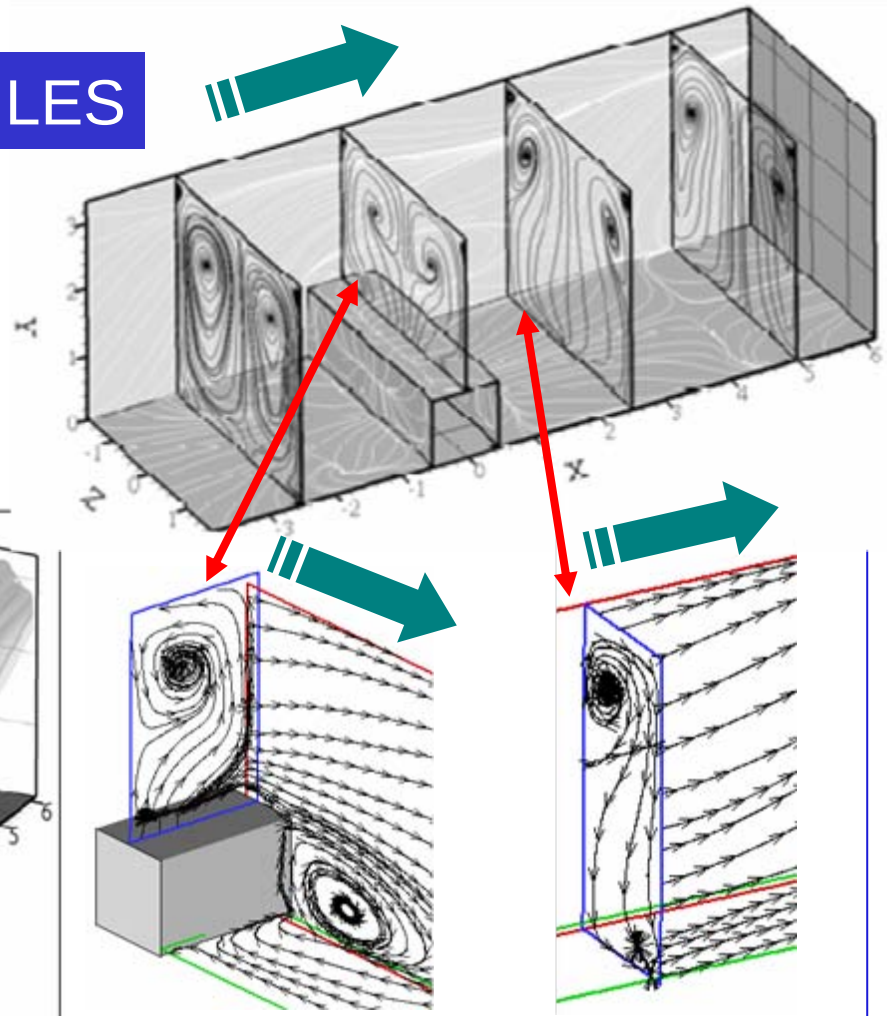

LES

PIV

Heat transfer over a single rib

Problem in Fluent when using:

Periodic condition + Heat transfer + Unsteady solver

The temperature is fixed in cell number 1 for several time step (thermal balance).

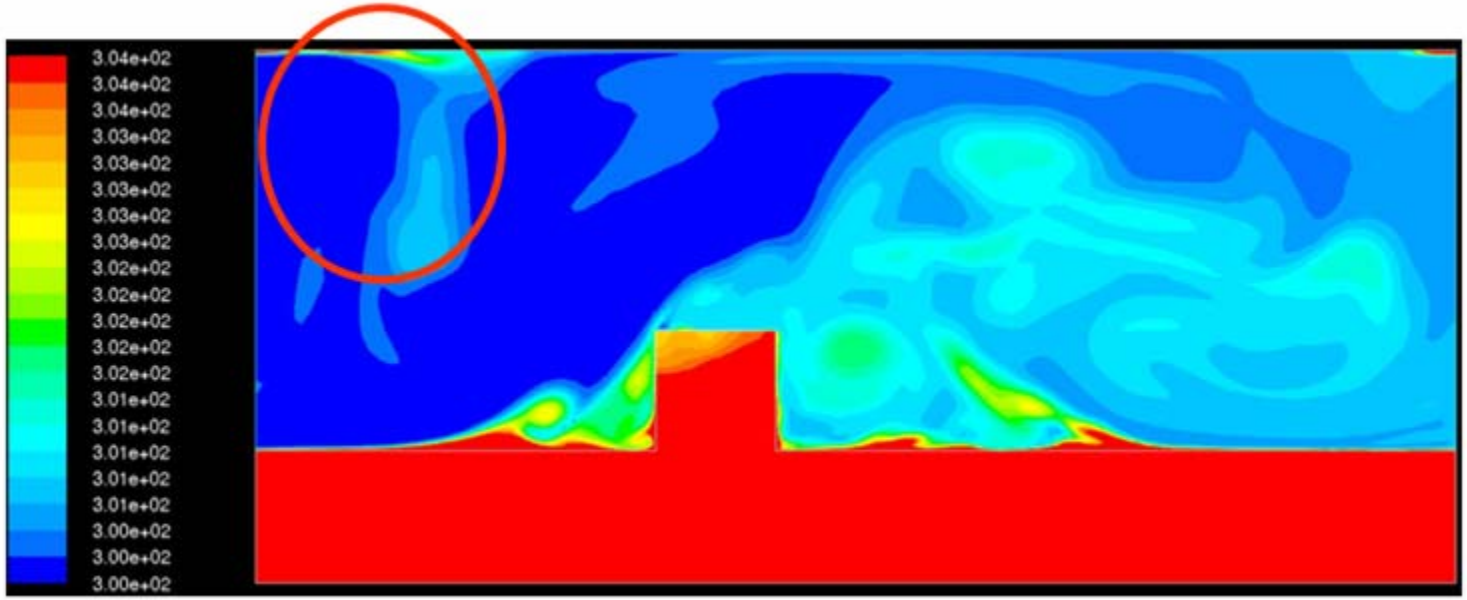

Periodic conditions have to be avoided.

Use of the single rib to generate mean BC

- ✓ The periodic simulation over 1 rib provides a time averaged inlet BCs.
- ✓ We will have to face the difficult problem of ‘open’ boundaries in LES
  => we need to provide a physical turbulent contents.
- ✓ What about inserting some ribs that will generate the correct turbulent contents
  => 3 ribs configurations

Computational domain and boundary conditions

- ✓ A RANS (realizable k-ε) simulation with conjugate heat transfer is done over 3 ribs to have an initial field for the LES.
- ✓ The full LES simulation over 3 ribs is done.

No-diffusion flux outlet bc.

Inlet profiles:

- Velocity components from periodic solution + perturbations
- Temperature from periodic solution

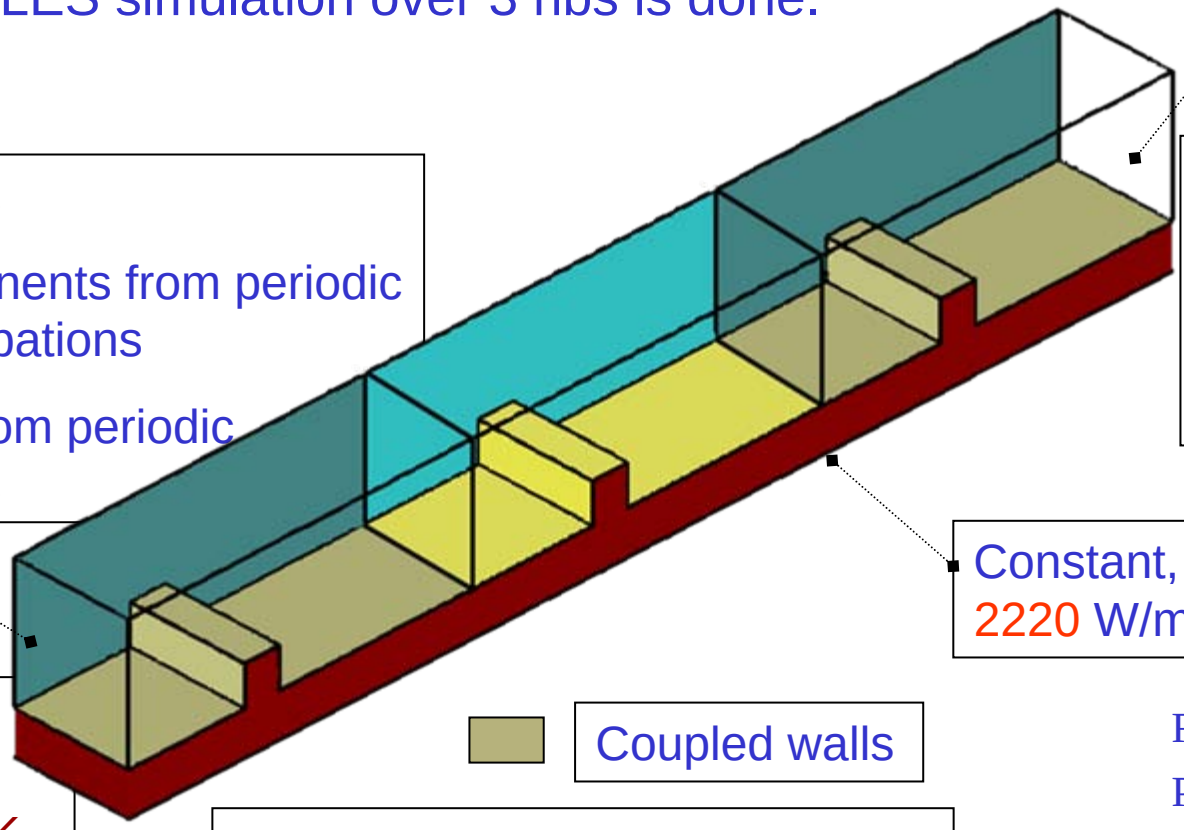

Fluid (air):
- $\rho = 1.225$ kg/m^3
- $c_p = 1006.43$ J/kgK
- $k = 0.0242$ W/mK
- $\mu = 1.79\times10^{-5}$ Pas

Constant, uniform heat flux:
2220 W/m^2

Solid (steel):
- $\rho = 8030$ kg/m^3
- $c_p = 502.48$ J/kgK
- $k = 16.27$ W/mK

Coupled walls

Rest of the walls are considered adiabatic

$$Re = 40000$$

$$Pr = 0.7$$

$$\frac{Gr}{Re^2} = 1.4\cdot10^{-3}$$

The mesh

Unstructured mesh in the X-Y plane:

- Structured blocks at the walls
- Refined around the second rib

Structured in the Z direction

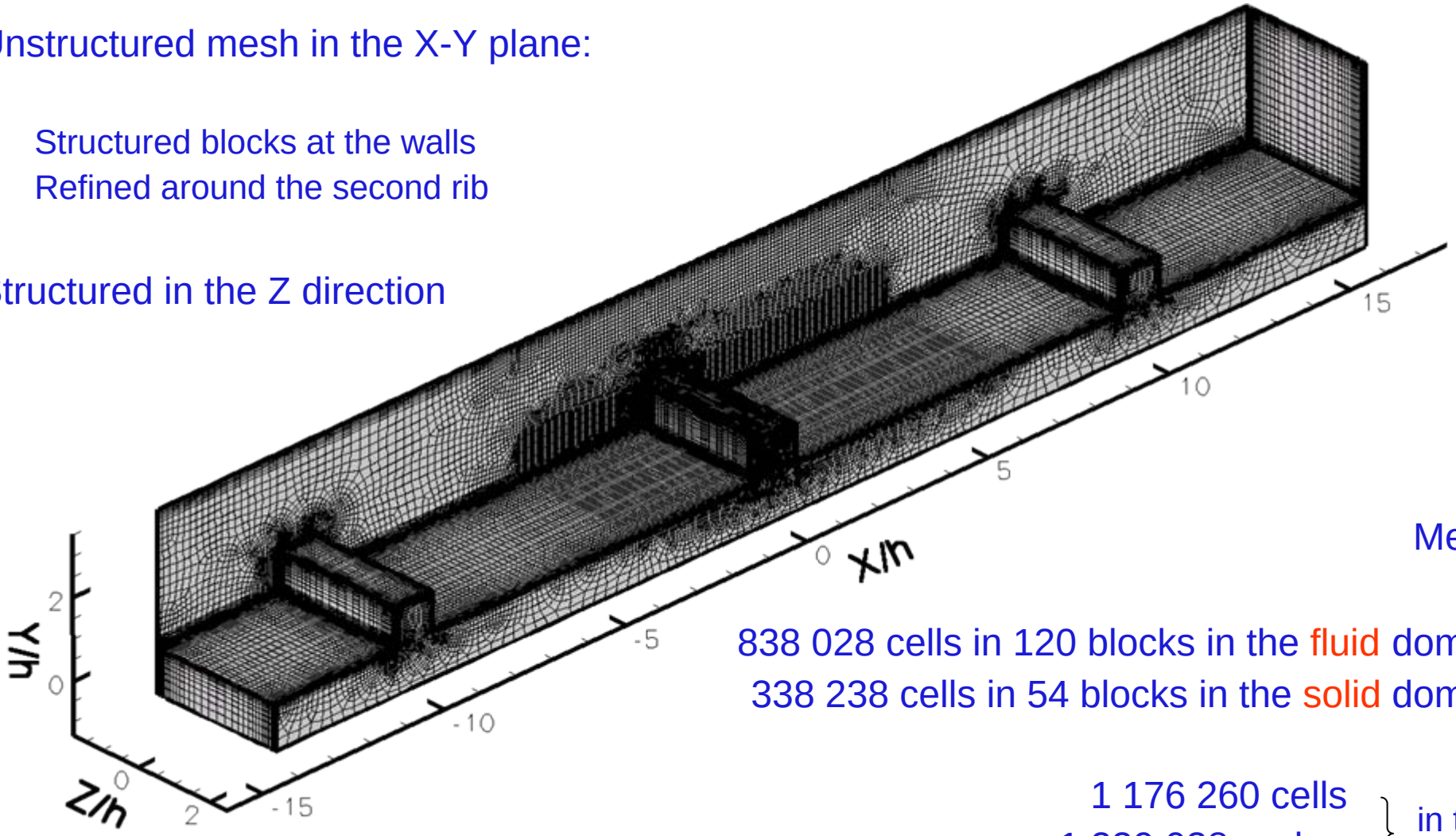

Mesh:

838 028 cells in 120 blocks in the fluid domain
338 238 cells in 54 blocks in the solid domain

1 176 260 cells
1 239 038 nodes
} in total

Numerical parameters

- Momentum interpolation: Bounded Central Differencing
- Pressure interpolation: Standard (second order)
- Pressure velocity coupling: SIMPLE
- Time discretization: Second order implicit
- Turbulence model: Smagorinsky-Lilly with $C_S = 0.1$
- Under-relaxation factors:
  - Pressure : 0.6
  - Momentum : 0.7
  - Energy : 1
- Convergence criterion:
  - 20 iteration steps
  - 2×10^{-5} for the scaled residuals of continuity
- $T_{ts\text{-}Ro=0} = 3\times10^{-5}$ s $= 3.98\times10^{-3}$ D/U_b ➡ 200s CPU time (no //)

Results of flow-field simulation

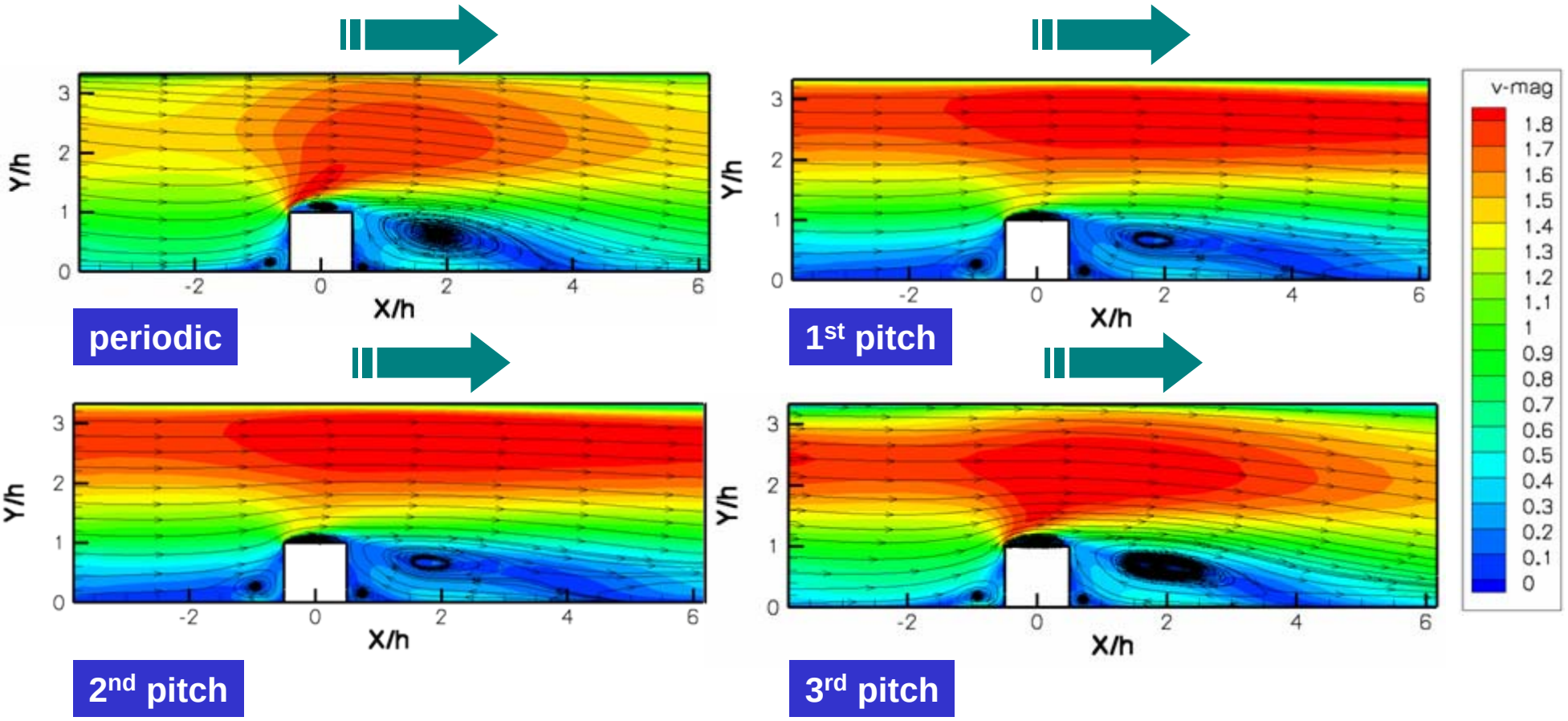

Contours of mean velocity magnitude with streamlines in the X-Y plane in the symmetry plane of the duct. After only the 3rd rib we start to retrieve the periodic results!!

Results of flow-field simulation

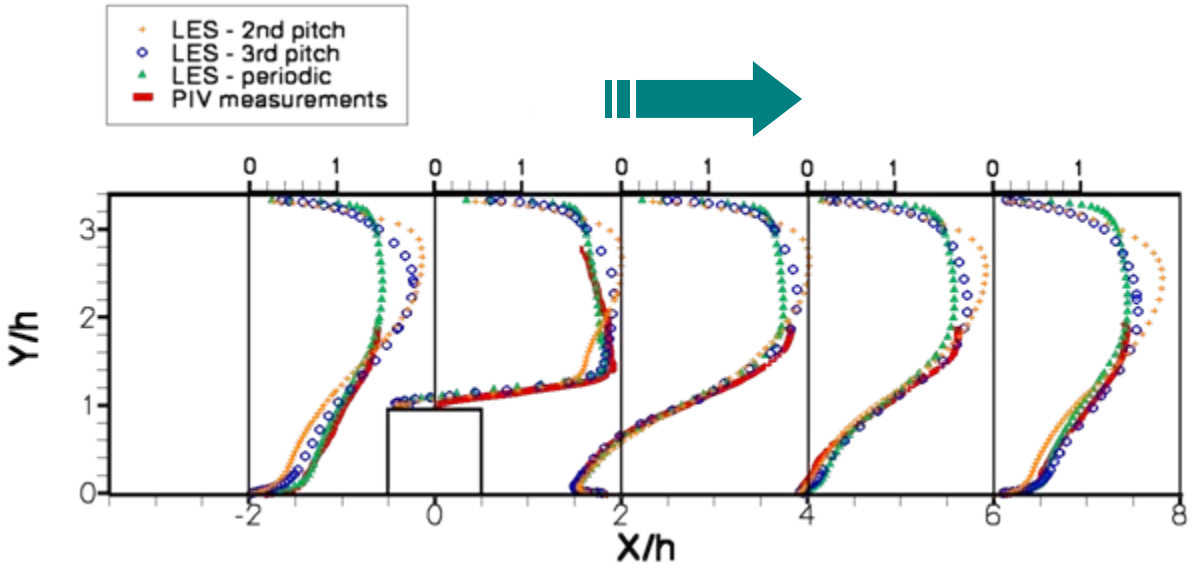

Profiles of the mean streamwise velocity component

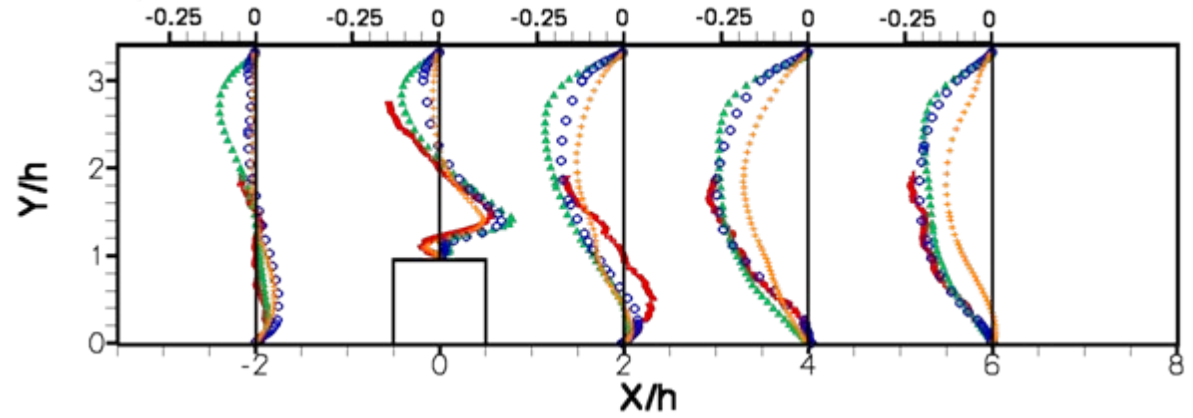

Profiles of the mean vertical velocity component

Results of flow-field simulation

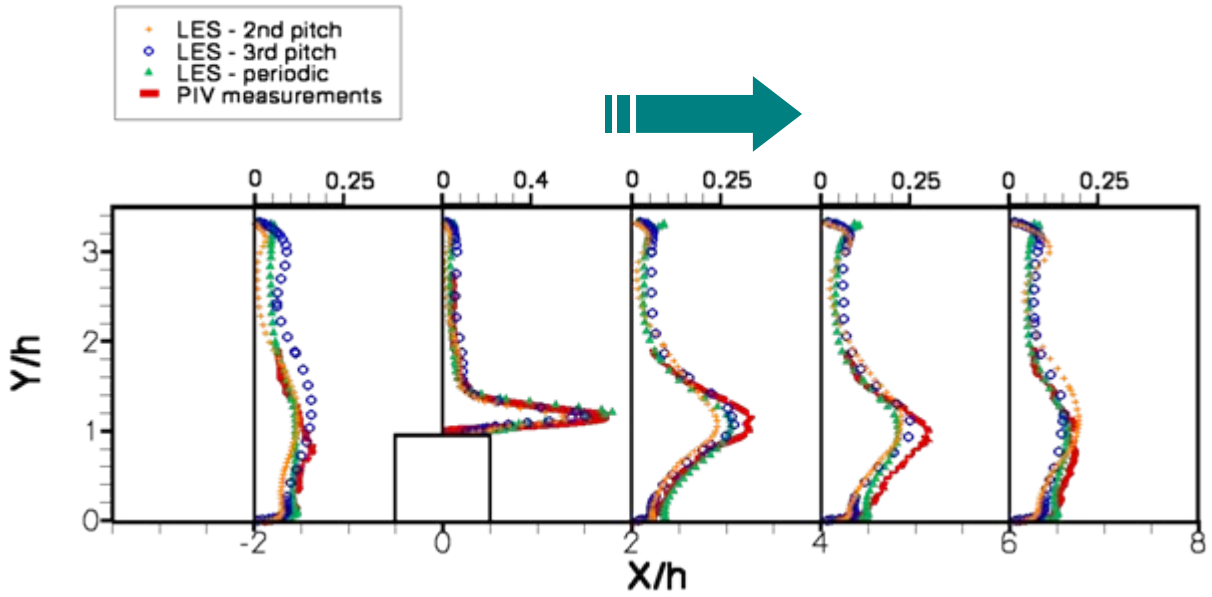

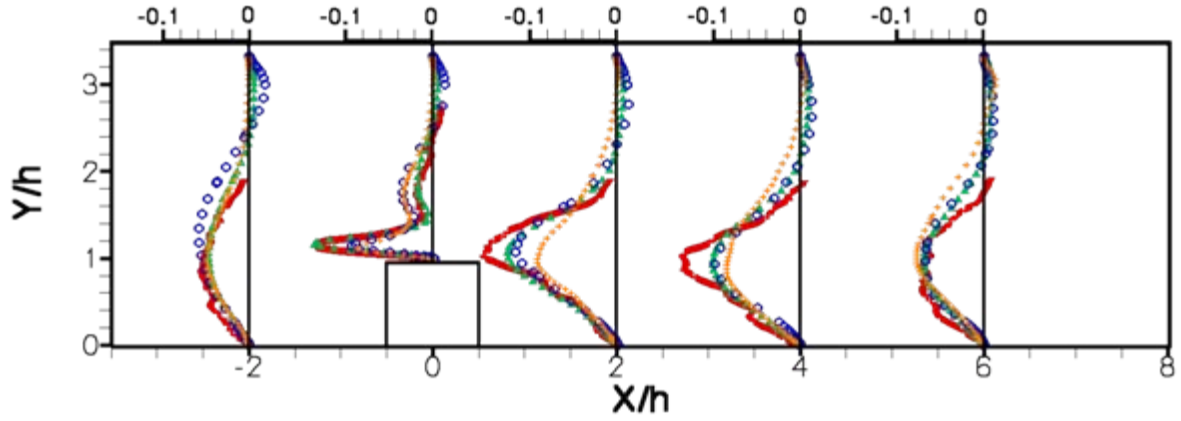

Profiles of the variance of the streamwise velocity component - <u'u'>

Profiles of the covariance of the streamwise and vertical velocity components - <u'v'>

Conclusions about flow-field simulation

- The flow is not fully periodic at the second rib
- The mean velocity components show a good agreement with the measurements after the 3rd rib
- Pressure drop over the 3rd rib matches measurements well
- Further extension of the numerical domain is proposed

$$f = \frac{D_H \Delta p}{2 l \rho U_b^2}$$

$$f_0 = 0.046\,\mathrm{Re}^{-0.2}$$

	f/f_0
Measurement :	12.3
LES with periodic bc. (C_S = 0.1) :	12.147
LES with inlet-outflow bc. (3rd pitch):	12.154

Definitions for heat-flux evaluation

Map of temperature field

in the symmetry plane from CFD

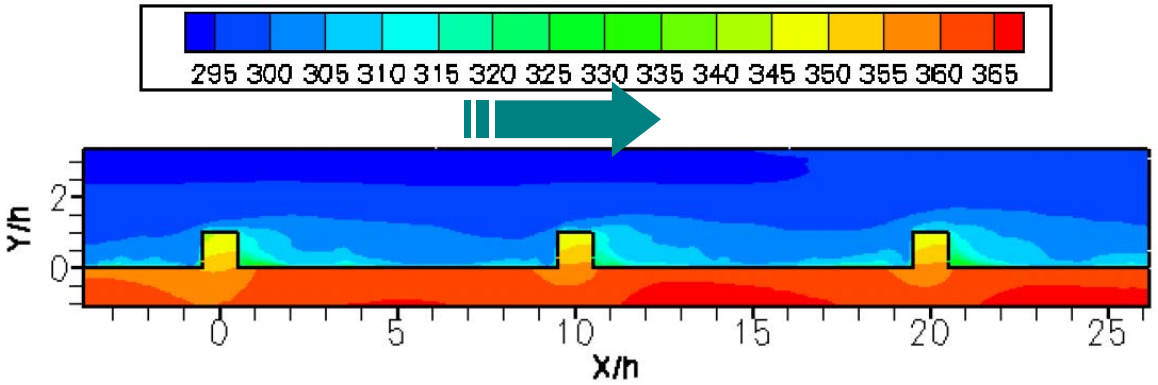

Local Nusselt number:

$$Nu = f(Re, Pr) = \frac{h(x_i)D_h}{k_{air}}$$

Nusselt number in smooth duct:

$$Nu_0 = 0.023 Re^{0.8} Pr^{0.4}$$

Enhancement factor:

$$EF = \frac{Nu(x_i)}{Nu_0} = \frac{\dot{q} D_h}{0.023 Re^{0.8} Pr^{0.4} (T_w - T_b) k_{air}}$$

Heat transfer coefficient:

$$h = \frac{\dot{q}}{T_w - T_b}$$

Results of heat transfer simulation

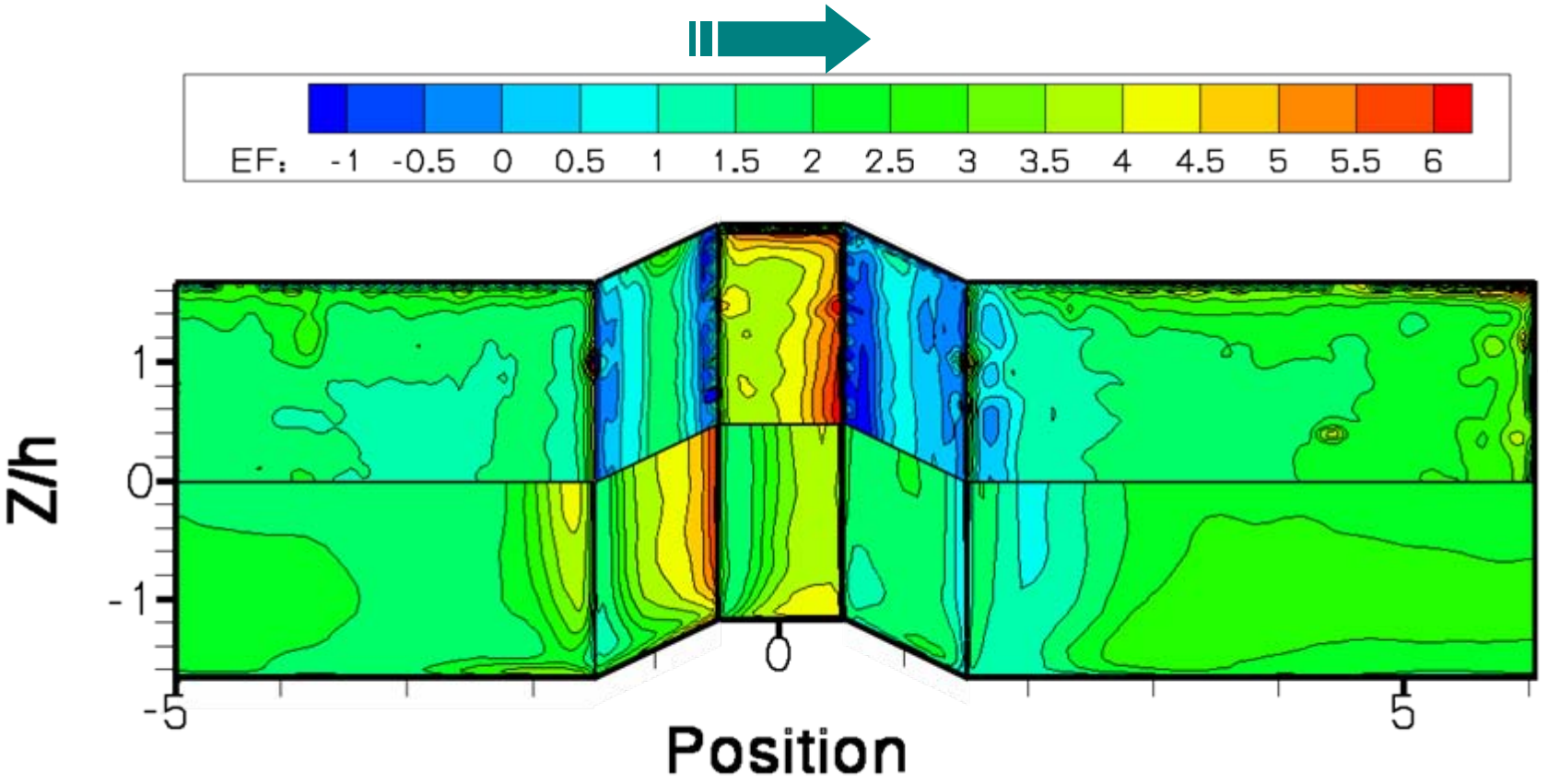

IC + inverse PB

LES

Contours of enhancement factor: “measured” (upper) and LES (lower).

Still work to be done one the experimental determination of EF on the Rib!

Conclusions

- Flow-field
  - Application with LES of the inlet-outlet boundary is successful but the flow gets periodic only after the third rib (bad turbulent contents in the inlet).
  - The use of extended domain is considered.
- Heat transfer
  - Computation shows good agreement with measurements on the bottom of the channel
  - Significant differences on the sides of the rib itself (determination of experimental heat flux from solid to air with inverse method has to be improved).

Future work

- Instantaneous analysis of the CFD fields (how the turbulent structures extract heat from solid).
- CFD of different ribs/duct geometries.
- Same study in rotating channels.